**Article:**
Longhi, M.A., Walkley, B., Rodríguez, E.D. et al. (2019) New selective dissolution process to quantify reaction extent and product stability in metakaolin-based geopolymers. Composites Part B: Engineering, 176. 107172. ISSN: 1359-8368

https://doi.org/10.1016/j.compositesb.2019.107172

# New selective dissolution process to quantify reaction extent and product stability in metakaolin-based geopolymers

Márlon A. Longhi[a, b*], Brant Walkley[c], Erich D. Rodríguez[d], Ana P. Kirchheim[a], Zuhua Zhang[b,e] and Hao Wang[b]

[a]Building Innovation Research Unit, Federal University of "Rio Grande do Sul" (NORIE/UFRGS), Av. Osvaldo Aranha, 99. 3[o]andar, Porto Alegre, Brazil. marlonlonghi@gmail.com

[b]Centre for Future Materials, University of Southern Queensland, Toowoomba, QLD 4350, Australia.

[c]Department of Materials Science and Engineering, Sir Robert Hadfield Building, The University of Sheffield, Sheffield S1 3JD, United Kingdom.

[d]Department of Structures and Civil Construction. Technology Centre, Federal University of Santa Maria, Santa Maria, Av. Roraima 1000. Prédio 7. RS, Brazil.

[e]Key Laboratory for Green & Advanced Civil Engineering Materials and Application Technology of Hunan Province, College of Civil Engineering, Hunan University, Changsha 410082, PR China

**ABSTRACT**

A selective dissolution process is developed that can quantify the amount of soluble material, geopolymer gel and remnant unreacted precursor in metakaolin-based geopolymer systems and determine the nanostructural features of the raw materials and geopolymer gel components. The susceptibility of alkalis leachability from the alkaline aluminosilicate hydrate-type gel (N-A-S-H) produced during the geopolymerization is not fully understood. This phenomenon led to deleterious processes from a microstructural, aesthetic and performance point of view. Geopolymers were synthesised using different contents and types of alkalis (M/Al=0.50-0.83, where M represents Na or K), different contents of soluble silica in the activator (expressed as $SiO_2/M_2O$ ratio of 1.0, 0.5 and 0.0), and curing temperatures (25 and 50ºC). The selective dissolution process is based on neutral

dissolution at pH 7 to extract the soluble materials and acid dissolution using a strong acid at pH 0 to dissolve the geopolymer gel, which provides for the first time a method to quantify the (i) soluble material, (ii) geopolymer gel and (iii) unreacted material in geopolymers. The soluble material provides a reliable indication of the materials that can be removed from the geopolymers in a neutral pH environment and hence the potential for leaching and efflorescence, which is useful for durability prediction and service life. Quantification of remnant unreacted metakaolin determines the reactivity of the precursor and assesses the suitability of different synthesis conditions for varied applications. This work therefore provides a novel and widely applicable approach to determine the susceptibility of geopolymer materials to leaching.

**KEYWORDS:** Alkali activation; geopolymer; aluminosilicate; leaching.

## 1. INTRODUCTION

The development of chemically activated reactive aluminosilicate materials has become a technically [1–3] and environmentally [4–6] attractive option for the use of different industrial wastes and calcined clays in manufacturing new binders. These are known as alkali-activated materials (AAMs) or geopolymers. Among the precursors used for geopolymer manufacturing, metakaolin is one of the most commonly used because of its high reactivity and purity, which result in a more homogeneous raw material and binder [2].

The main reaction product formed in geopolymers is an alkaline aluminosilicate hydrate type-gel (also known as M-A-S-H, where M represents the alkali metal in activator). The alkali metal most commonly used and assessed is sodium, which promotes formation of a structurally disordered and highly cross-linked N-A-S-H gel [7]. When metakaolin is used as the precursor, Al and Si in the M-A-S-H gel structure are present in tetrahedral coordination, with silica in a $Q^4(m\text{Al})$ ($0 \leq m \leq 4$) type environment [8]. Aluminium plays an important role in the process of dissolution, crystallisation and reaction product formation [2]. Aluminium also influences the intrinsic mechanical properties, where large amounts of $Q^4(3\text{Al})$ and $Q^4(2\text{Al})$ sites (resulting from a relative increase of Si in the system) provide higher strength to the gel structure than $Q^4(4\text{Al})$ sites [9].

The composition and quantity of the M-A-S-H gel formed during geopolymerisation is dependent on the degree of reactivity of the precursor, which itself is related to the reactive oxide content, chemical composition and particle morphology. The high pH provided by the activator facilitates the dissolution Al and Si from the precursor particles, which then precipitate and polymerise via condensation reactions to form the geopolymer gel. During the initial stages of reaction dissolution of Al-O bonds is thermodynamically more favourable than dissolution of Si-O bonds [9],[10], indicating a higher initial reactivity for alumina rich precursors. The use of soluble silicates in the activator provides an extra source of silica to the system and induces the incorporation of Si in the gel structure and the subsequent formation of Si-rich tetrahedral sites. The presence of excess alkalis from the activator can facilitate leaching and subsequent efflorescence formation [11] and changes in the durability of the material due to mechanical performance reduction [12–14]. The type of alkali affects

precursor dissolution kinetics and therefore the microstructure of the final product. In this sense, the synthesis parameters are determinants of gel formation, chemical composition, microstructural features and durability.

Regarding the behaviour of alkalis in the gel structure, sodium can be present as Na-O-Al(Si) or as $Na(H_2O)_n^+$, weakly associated with water molecules [10,11]. The weak bonding or availability of alkalis in the aqueous phase present in the gel pore network increases the materials susceptibility to leaching. Previous work has shown leaching of between 1 and 16% of alkalis from the gel during the first 24 hours of exposure [17,18], and it has been suggested that complete dissolution is likely after a long exposure time [14,15]. The wide variation in leaching behaviour in those studies is due to substantially different geopolymers made using materials (fly ash and calcined clay) exhibiting very different chemical composition and mineralogy, under distinct activation and exposure conditions.

Considering all of these factors, determination of the reaction extent is therefore critical for the synthesis of geopolymer gel composition prediction of long-term mechanical properties, chemical and physical durability. The most important synthesis parameter in formulating geopolymer reaction mixtures is the Na/Al molar ratio, where the unit value indicates the extent of compensation of the negative charge resulting from the substitution of Al into a $Q^4$ molecular coordination [7,9]. However, due to the difficulty in identifying the degree of reaction of the precursor (and/or the Al dissolution degree in alkaline environment), and the amount of gel formed, this value is typically calculated by assuming that the total amount of Al in the precursor is incorporated into the gel framework and exists in a $Q^4$ environment. In practice this is unlikely to occur, as much of the Al will remain in unreacted precursor particles or crystalline phases that are inert under the reaction conditions of alkali activation (e.g. mullite in coal fly ash) [21]. In this case, excess of Na remains free in the gel pore solution. However, increasing of reaction mixture pH by the addition of greater amount of Na (i.e. increasing the activator dose) results in greater dissolution of the precursor and consequently more gel formation. This results in a greater charge balancing requirement and hence greater incorporation of alkalis in the gel. There exists an optimum point between maximum particle dissolution and a minimum amount of free alkalis in the pore solution, in regard to the long-term mechanical properties, chemical and

physical durability. It is therefore necessary to understand how the different design parameters influence the degree of reaction of the precursor and how the removal of free alkalis can affect the composition and stability of the gel. In this sense, the free and/or weak bonding alkalis increase the potential of deleterious phenomena related to efflorescence development. The mechanical and physicochemical properties (e.g. chemical durability and permeability) of the geopolymers result from the gel reaction product, and this may be estimated from the reacted portion of the precursor which is not soluble [21,22]. Consequently, the degree of reaction during geopolymer formation is fundamental to understand and predict reaction mechanisms and kinetics and mechanical and physicochemical properties in geopolymer systems.

This degree of reaction in geopolymer systems has been assessed in previous work using varying approaches, with chemical methods of selective dissolution and analytical methods of quantification yielding the most promising results. The reactivity of fly ash was evaluated by alkaline dissolution and analytic quantification using X-Ray Diffraction (XRD) and X-Ray Fluorescence (XRF) [23]. In a complementary approach, the reaction extent of fly ash and/or slag based geopolymers was evaluated by selective dissolution and thermogravimetric analysis (TGA), nuclear magnetic resonance (NMR) spectroscopy and scanning electron microscopy (SEM) [24,25]. The degree of reaction of slag in blended Portland cement was assessed using selective dissolution based on ethylene diamine tetra acetic acid (EDTA) extraction coupled with $^{29}$Si MAS NMR [26,27]. The extent of reaction of metakaolin-based geopolymers was evaluated using XRD (Area Ratio Method (ARM) and Partial or No Known Crystal Structure (PONCKS) methods), SEM and Energy-dispersive X-ray spectroscopy (EDS) [22].

Despite the valuable contributions that this work has made to the understanding of the reaction extent in geopolymer systems, some points remain unclear. In particular, a detailed understanding of the effect on gel formation of the alkali and soluble silicate content in the reaction mixture remains absent from the literature, as does its relation with the amount of readily soluble, poorly soluble and insoluble components of the geopolymer gel and remnant unreacted material within the binder. These parameters could be useful to make a correlation between the reaction mechanisms and kinetics of gel

formation, as well as resistance to degradation in aggressive environments, and therefore have significant implications on geopolymer durability and performance.

In the present work a carefully designed selective dissolution process was used, which is coupled with microstructural and spectroscopic techniques probing phase assemblage and nanostructure, to quantify the amount of soluble material, geopolymer gel and unreacted precursor in Ca-free geopolymer systems. This can quantify and assess the susceptibility of geopolymer materials to leaching (or efflorescence development). The reaction extent of a set of metakaolin-based geopolymers produced using different synthesis conditions (different activator content, soluble silicate content, type of alkali, and curing conditions) is assessed, where the results obtained are related with material stability, as well as the microstructural and nanostructural changes derived from the selective dissolution process. This provides new insight about the reaction product formed in metakaolin-based geopolymers, the state of alkalis in the structure and the nature of the selective dissolution processes, knowledge that is essential to define the design parameters and predict the durability of geopolymers materials.

## 2. EXPERIMENTAL PROGRAM

### 2.1 Materials and sample preparation

A commercial metakaolin (MetaMax – BASF) was used as the aluminosilicate precursor, with a mean particle size of 4.56 μm and a specific surface area of 13.49 m²/g. This material showed a smaller particle size than other calcined clays [28,29], which might result in higher water consumption during geopolymer production. The properties and chemical composition are shown in Table 1.

Activating solutions were produced from analytical grade sodium hydroxide pellets (NaOH: ~99%, Chem-Supply, Australia), analytical grade potassium hydroxide pellets (KOH: ~85%, Chem-Supply, Australia), both dissolved in water, and a sodium silicate solution with 29.4 wt.% $SiO_2$, 14.7 wt.% $Na_2O$, and 52.7 wt.% $H_2O$, supplied by PQ Australia.

The geopolymers were formulated with different contents of alkali activator ($M_2O$= 15, 20 and 25%). If metakaolin is assumed to react fully, the final M/Al ratios are between 0.5 to 0.83. The type and content of alkalis were selected according to the literature in order to have a wide range of design parameters [11,17,28]. Activating solutions were designed to give the content of silica in the activator (expressed as MS modulus, representing $SiO_2/M_2O$ molar ratio) as 0.0, 0.5, and 1.0. The alkali activators were produced by blending the NaOH/KOH and sodium silicate solution in proportions to achieve the desired molar ratios. The geopolymer formulations are identified by codes as follows: "Type of activator and curing temperature [content of alkali](MS modulus)". For example, the system "Na[20](1.0)" was activated using 20% $Na_2O$, at room temperature, with a MS modulus of 1. The mixes are listed in Table 2. To assess the effect of thermal curing, the systems activated at 20% of $Na_2O$ with different MS were also cured at 50 °C for 24 h. This curing process was made with the samples sealed inside a hermetically sealed box with water in the bottom, without contact with the samples. This process was made to avoid the loss of water by evaporation.

The pastes were produced by mechanically mixing the activator and metakaolin precursor for 5 min (1 min at 140 rpm and 4 min at 280 rpm) and then pouring the resultant mixture into moulds. Cubic samples with a height of 20 mm were produced for compressive strength testing. All the samples were cured at either 25 °C or 50 °C for 24 hours and then stored in a sealed plastic container at room temperature (~25 °C) and RH ≥ 90% for 28 days.

2.2 Tests conducted

The compressive strength of each hardened sample was measured at 28 days using an MTS universal mechanical testing machine with a loading speed of 0.5 mm/min.

The selective dissolution tests involved dissolving the sample under different pH conditions and assessing the remaining material by micro and nanostructural analysis. The selective dissolution was divided into two different stages:

- Part 1, denoted as **process WD** (water dissolution): Extraction of soluble materials in a neutral pH environment. Two grams of ground hardened binder (passed through a 75 μm

sieve) was immersed in 200 g of distilled and deionised water. The solution was stirred using a magnetic stirrer for 5 minutes the pH measured and adjusted to a neutral value of pH = 7 through the addition of HCl (36 vol. %) to neutralise any dissolved alkalis. This process was repeated 5 times until the pH of the solution remained stable (i.e. no further observable dissolution of alkalis occurred), with the quantity of HCl added recorded. The solution was then filtered using a quantitative filter and the extracted solid material was then rinsed once with distilled water, and subsequently rinsed twice with ethanol. The remaining solid material was then dried for 45 minutes in an oven at 40 °C and collected for analysis.

- Part 2, denoted as **process AD** (acid dissolution): Dissolution of reaction products by acid attack. One gram of hardened ground geopolymer was immersed for one minute in 100 g of deionised water while stirring using a magnetic stirrer, to which 50 ml of HCl (36 vol. %) was then added while stirring using a magnetic stirrer for another 29 minutes. The solution obtained was then filtered as described above, and the remaining (inert) solid material was collected for analysis.

The geopolymers and the filtered solid material obtained from the selective dissolution processes WD and AD were analysed by:

- X-Ray Fluorescence (XRF) using a Panalytical Axios instrument, with a resolution (Mn Kα) of 35 eV, using wavelength dispersive X-ray fluorescence.
- Solid-state single pulse $^{27}Al$ and $^{29}Si$ magic angle spinning (MAS) NMR spectroscopy using a Bruker Avance III HD 500 spectrometer at 11.7 T ($B_0$) with a 4.0 mm dual resonance CP/MAS probe, yielding a Larmor frequency of 130.32 MHz for $^{27}Al$ and 99.35 MHz for $^{29}Si$. $^{27}Al$ MAS NMR spectra were collected with a 1.7 μs non-selective (π/2) excitation pulse, a measured 5 s relaxation delay, a total of 512 transients and spinning at 12.5 kHz. $^{29}Si$ MAS NMR spectra were acquired using a 5.5 μs non-selective (π/2) excitation pulse, a measured 60 s relaxation delay, a total of 256 transients and spinning at 12.5 kHz. For all experiments, the spectrometer field was aligned to the $^{13}C$ resonance of adamantane at 38.48 ppm, and $^{27}Al$ and $^{29}Si$ spectra were referenced to 1.0 mol/L $Al(NO_3)_{3(aq)}$ and neat tetramethylsilane (TMS),

respectively, at 0 ppm. Gaussian peak profiles were used to deconvolute the NMR spectra, using the minimum number of peaks possible [30]. Peak intensities were required to be consistent with the structural constraints described by the thermodynamics of a statistical distribution of Si and Al sites within a $Q^4$ aluminosilicate network for (N,K)-A-S-H gel products [31].

- X-ray diffraction (XRD) using a Bruker D2 Phaser instrument with Cu Kα radiation, a nickel filter, a step size of 0.020° and 0.5 s/step. Data was obtained in the range from 5 to 70° 2θ. Diffracted background intensity at low angles was reduced using an anti-scatter blade, an incident beam divergence of 0.6 mm and a 2.5° Soller slit in the diffracted beam. Phase analysis was performed using X'Pert High Score Plus software with the ICDD PDF-4+ 2016 database.
- Fourier Transformed Infrared Spectroscopy (FTIR) using a Perkin Elmer FTIR-ATR spectrometer in absorbance mode from 4000 to 400 $cm^{-1}$. Using absorbance values, the spectra were fitted using a baseline correction and deconvoluted in the range of 600 – 1300 $cm^{-1}$ using Gaussian curves, with the baseline defined and the band position and shape assigned according to the literature [28,32].
- Scanning electron microscopy (SEM) using an EVO MA18 40XVP instrument, with an accelerating voltage of 10 kV. The samples were dried at 60 °C for 2 hours and coated with gold prior to analysis.

## 3. RESULTS AND DISCUSSION

### 3.1 Compressive strength

The compressive strength results of the geopolymers with different synthesis parameters are shown in Figure 1. Increasing soluble Si content in the activator (provided by sodium silicate) results in a significant increase in compressive strength. The system with MS=1 presents values up to 3.3 times higher compared to MS=0 (sodium hydroxide-based systems). This increasement is related to the formation of a denser and more compact geopolymer structure with the use of an activator rich in

soluble silicate providing compressive strength values close to 45 MPa for the geopolymer samples investigated here. This behaviour is aligned to previous reports [9,11,28].

An increase in reaction mixture sodium content also results in an increase in compressive strength. The geopolymers with 25% of $Na_2O$ (Na[25]) exhibit compressive strength values up to 1.2 times higher compared with $Na_2O$ of 20% (Na[20]) and 2.5 times higher when compared with $Na_2O$ of 15% (Na[15]). The increasing in the amount of soluble silicate associated with the alkali content can provide a higher precursor dissolution, more gel formation and higher compressive strength [33,34].Using potassium as the alkali source results in lower compressive strength values than those observed for samples based on sodium (considering the alkali content and MS parameters being equal). Curing at 50 °C results in a reduction in the compressive strength of the MS>0 systems and a slight increase in the compressive strength of the NaOH-based geopolymers when compared with those samples cured at 25 °C.

3.2 Selective dissolution

The results of each selective dissolution process are shown in Figure 2. The selective dissolution process WD (part 1) determines the content of soluble material at pH 7. The elements in chemically stable atomic bonds are generally not be removed in a neutral environment. The selective dissolution process WD (part 1) showed that the metakaolin precursor is insoluble at pH 7, while the aluminosilicate framework formed in metakaolin-based geopolymers is largely hydrolytically stable, due to the high $SiO_2/Na_2O$ of aluminosilicate gel formed, in agreement with other researches [35,36], which means that the dissolved material in each sample can be attributed primarily to alkalis leaching from the reaction products, or unreacted alkalis from the pore solution. The soluble alkali content of the system will therefore be proportional to the extent of dissolution at pH 7. Samples with MS=0 (i.e. without any soluble silicate present in the activator) produced from KOH-based activators exhibited a lower extent of dissolution compared to that of samples with MS=0 produced from NaOH-based activators. Curing at 50 °C results in a slight increase in soluble material within the geopolymer, the extent of which is more pronounced as the amount of soluble Si in the reaction mixture is decreased. The selective dissolution process WD was applied to finely ground material and consequently the

dissolution of soluble material (i.e. alkalis) is faster than the geopolymer gel framework. This is due to the higher surface area and reduced tortuosity of the pore network (and hence the easier release of Si, Al, and alkalis in the pore solution) of the powdered samples. As the potential for efflorescence is directly related to the extent to which alkalis are leached from geopolymer materials, the solubility of ground geopolymer samples in a neutral pH environment provides a reliable indicator of the potential for efflorescence and oxide removal.

In acid dissolution (process AD), the powdered geopolymer was immersed in a concentrated HCl solution to dissolve all the M-A-S-H gel such that the remaining insoluble fraction obtained can then be attributed solely to the unreacted precursor. The metakaolin precursor was treated under the same conditions, and the solubility was shown to be negligible as shown in the first column of Figure 2. The results in Figure 2 show that higher content of $Na_2O$ leads to greater gel formation (i.e. comparing the systems Na[20] and Na[15]). Greater gel formation is also identified at higher values of MS regardless of the $Na_2O$ content. The use of potassium as part of activator results in lower gel formation (consistent with the compressive strength values for these samples), and in the system Na+K[20](0.0) the content of geopolymer formed is only ~30% (c.f. 56% for the system Na[20](0.0)). No significant differences were identified between systems cured at 25 ºC and 50 ºC.

The quantity of gel formed in each sample determined from the dissolution processes can be used to elucidate the reaction extent of the geopolymers, and related to the mechanical properties, where more content of gel induces the formation of a more compact structure and consequently with more strength and lower permeability [22]. The data in Figure 2 show that the type of activator (nature of alkali cation and the presence of soluble silicates) and its concentration (%$M_2O$) used for geopolymer synthesis have a strong influence on the gel structure. Despite the complex phase assemblage and microstructure (discussed in further detail below), a direct relationship between compressive strength and gel formation is observed. Systems with greater MS values showed higher gel formation and compressive strength values when activator content and type are held constant, and systems with greater activator content showed higher gel formation and compressive strength value when MS values and activator type are held constant. Additionally, systems with sodium as the alkali source

show higher gel formation and compressive strength values compared to systems where both sodium and potassium are used as the alkali source. The equivalent content of $M_2O$ results in a visible reduction of the compressive strength and gel formation when using hydroxide as the activator rather than soluble silicate. A notable example of this is the system Na+K[20](0.0) which exhibits gel formation of 30.7 wt.% (relative to the total geopolymer mass), yet a compressive strength of less 0.8 MPa. From Zhang et al. [28], this extremely low strength is related to the highly porous structure and weak binding property of the gel. Additionally, according to Duxson et al.[37], the mechanical properties on K-based systems is also dependent on Si/Al molar ratio, where low levels indicate lower reactivity. This trend is observed for all systems in which potassium is used as an alkali source, also indicating greater effectiveness for systems with higher Si content in the reaction mixture.

The results above show that selective dissolution process allows identification of the soluble, insoluble and gel materials. The susceptibility of geopolymers to efflorescence is related to the leaching characteristics, in particular the specific constituents that are leached from the material. For this reason, it is necessary to identify what constituents are being released in a neutral pH environment (process WD).

Figure 3 shows the $SiO_2$, $Al_2O_3$ and $Na_2O$ content, determined using XRF, in the remaining solid phase obtained from the two selective dissolutions processes for the geopolymer systems with 20% of $Na_2O$.

The composition of the dissolved materials shows a large extent of sodium being released, in some cases even greater than 50% of the nominal sodium content, which indicates that a large fraction of sodium is not chemically bound in gel or is weakly bound and is free to move in a neutral pH aqueous environment. The high amount of free sodium in the structure is an indicator of potential efflorescence formation when geopolymers are under high humidity conditions.

The quantity of alkalis within the material dissolved in acid (i.e. the gel content) is 43-47 wt.% (Figure 3C) of the total amount of oxide, along with 54-70 wt.% $SiO_2$ and 63.5-69 wt.% $Al_2O_3$. The use of sodium silicate induces the greater formation of a silica-rich gel structure. The content of

alumina is relatively constant regardless of the synthesis conditions, and a low fraction (~3 wt.%) is leached at pH 7 (Figure 3B). The insoluble fraction is the remnant metakaolin precursor that is inert under acidic conditions, whose alumina and silica ratios are similar that of the original metakaolin, with a slight increase in the amount of silica. The sodium oxide content in the gel (Figure 3C) is less than half of the nominal sodium content in the initial geopolymer formulation (> 15% of $Na_2O$). The difference of initial geopolymer formulation and the composition of the resultant gel (oxide content from the filtered solid phase obtained in the acid dissolution) is shown in Figure 4, where it is possible to observe the removal of $Na_2O$ in the geopolymer structure.

Leaching of components during the selective dissolution process will result in changes to the chemistry (as shown above) and microstructure of the M-A-S-H gel, which will affect the physico-mechanical performance of the geopolymer materials. Therefore, the geopolymers were analysed in their original form (without any dissolution process), after dissolution in pH 7 (process WD) (to examine the gel content) and after dissolution in acidic conditions (process AD) (to examine the unreacted metakaolin). The microstructural analysis was performed for the representative systems Na[20](1,0), Na[20](0,5) and Na[20](0,0) and is discussed in the following sections.

3.3 XRD analysis

Figure 5 shows the XRD data for anhydrous metakaolin, the geopolymer samples after 28 days of curing and the samples obtained after each dissolution process. A broad feature due to diffuse scattering is visible between 15° and 35° 2θ in the XRD data for metakaolin, indicating its amorphous nature and hence high reactivity. The crystalline peaks observed in metakaolin are attributed to anatase ($TiO_2$, Pattern Diffraction File, PDF# 00-021-1272) and halloysite ($Al_2Si_2O_5(OH)_4$, PFD# 00-029-1489). In the metakaolin-based geopolymer samples, a broad feature between 20° and 35° 2θ is observed, indicating formation of an amorphous reaction product consistent with a M-A-S-H gel[11,28]. The crystalline phases identified in the unreacted metakaolin are observed in all geopolymers regardless of the synthesis conditions, indicating that these phases are inert under the assessed conditions. The ratio of the intensities of the broad feature at between 20° and 35° 2θ (attributed to M-A-S-H) and the broad between 15° and 35° 2θ (attributed to unreacted metakaolin) in

the XRD data for each geopolymer sample cured for 28 days increases with increasing soluble Si in the activator, indicating a greater reaction extent is promoted by increased soluble Si in the reaction mixture. This is consistent with the data from the selective dissolution processes discussed above.

After selective dissolution under acidic conditions (process AD), the intensity of the crystalline phases increases when related to the intensity of the broad feature and compared with the metakaolin XRD data. During the selective dissolution process, the amorphous M-A-S-H gel is consumed and the intensity of the broad feature due to this phase in the XRD data reduces, while the inert crystalline phases are not consumed, and hence the amount of these crystalline phases relative to the M-A-S-H gel increases, increasing the intensity of the reflections due to these phases in the XRD data. The Na[20](0.0) sample showed the formation of a zeolite phase exhibiting a Linde Type A structure (zeolite A, $Na_{96}Al_{96}Si_{96}O_{384}{\cdot}216H_2O$; PDF# 00-039-0222), which has also been observed in the use of in metakaolin-based geopolymers by Zhang et al.[28].

Examining the XRD data it is possible to observe the different microstructural transformations occurring during each selective dissolution process, mainly due to the AD process. During the selective dissolution process WD the removal of soluble elements (primarily Na, along with smaller amounts of Al and Si) were observed (Figure 3), however these did not result in any changes in the XRD data. The XRD patterns for the insoluble materials (after selective dissolution under acidic conditions, process AD) are very similar to that of anhydrous metakaolin, suggesting that the insoluble material comprises unreacted metakaolin. This verifies the efficacy and suitability of the selective dissolution method adopted here. Movement of the broad feature due to diffuse scattering in the XRD data for each geopolymer system to higher or lower values of 2θ after each dissolution processes suggests significant microstructural changes are occurring (discussed in further detail below). The zeolite phase (Z) was identified in Na[20)(0.0) (Figure 5C). Formation of zeolite phases is common in geopolymer systems contain nanocrystalline zeolites[7], and the formation of this phase is therefore unsurprising. After selective dissolution at pH 7 (process WD), the zeolite A phase is partially dissolved, which means that this phase is not stable, possibly due to low crystallinity or small grain size. Dissolution of zeolites at neutral pH conditions has been previously reported, and this can

result in degradation of the framework, partial dissolution of Si from the framework, and silicate precipitation[38,39]. A small peak at approximately 31° 2θ is observed in the XRD data for Na[20](1.0) (Figure 5A). This is consistent with the main reflection of magnesium iron oxide ($Fe_2MgO_4$, PDF# 00-036-0398), and is attributed to minor contamination during preparation of this sample.

3.4 Solid state MAS NMR spectroscopy analysis

The $^{27}$Al MAS NMR spectra of the anhydrous metakaolin precursor and geopolymer samples before and after each selective dissolution process are shown in Figure 6. Three broad resonances centred at $\delta_{obs}$= 6, 32 and 57 ppm are identified in the spectrum for anhydrous metakaolin, which are assigned to aluminium in tetrahedral (IV), pentahedral (V) and octahedral (VI) coordination. These Al species are usually present in approximately equal proportions due to the highly disordered nature of Al sites in metakaolin [8,40]. According to other authors, halloysite contains Al(VI) sites as the main Al environment [41–43] and will therefore, contribute to the intensity of the Al(VI) resonance in the $^{27}$Al MAS NMR spectrum for this sample. During the geopolymerisation process, Al(V) and Al(VI) within metakaolin dissolve and react to form Al(IV) species within the geopolymer binder [15]. This is consistent with the formation of the main $^{27}$Al MAS NMR resonance at $\delta_{obs}$= 60 ppm observed in this study. This resonance is assigned to Al(IV) in a $Q^4$ environment within a highly polymerised N-A-S-H gel framework [15,44]. Zeolite A in the system Na[20](0.0) will also contain Al(IV) environments [45,46], and these will contribute to the intensity in this region of the $^{27}$Al MAS NMR spectra for this sample. In addition to the main Al(IV) resonance, a low-intensity resonance at $\delta_{obs}$= 6 ppm is also observed in the $^{27}$Al MAS NMR spectra for each sample. This resonance has the same line shape as that observed in the spectra of metakaolin precursor and is therefore attributed to the presence of unreacted metakaolin Al(VI) species [40]. The ratio of the intensities of the Al(IV) and Al(VI) resonances (i.e. $I_{Al(IV)}/I_{Al(VI)}$) is greater as the soluble Si content in the activator (i.e. MS) is increased, indicating that the presence of soluble Si in the reaction mixture has promoted a greater reaction extent, consistent with observations from XRD and selective dissolution data discussed above.

After selective dissolution at neutral pH (process WD), a reduction in the intensity of the main Al(IV) resonance is observed for each sample. As shown in Figure 3, soluble Al and Si species are dissolved, and this reduces the relative amount of Al(IV) species present in the solid phase after dissolution. The intensity reduction becomes more pronounced as soluble Si content in the activator is decreased (i.e. moving from MS = 1.0 to MS = 0.5 to MS = 0.0), consistent with the decrease in nominal Si/Al of these samples and thermodynamic preference for dissolution of Al-O bonds[10], as well as previous findings that the amount of silica in the activator determines the speciation of aluminium during the reaction [8]. This intensity reduction as a consequence of the dissolution can be attributed to the removal of $Al(OH)_{4^{-}(aq)}$ in the gel pores [8] and the removal of weaker or less crosslinked Al species. An intensification of the resonance at approximately $\delta_{obs}$= 6 ppm is also observed after selective dissolution at neutral pH (process WD), which is due to the greater relative amount (and hence easier visibility) of the Al(VI) sites present in the anhydrous metakaolin precursor, which is inert under acidic conditions. This is consistent with the greater thermodynamic stability of Al(VI) when compared with Al(V) and Al(IV) [8].

The $^{27}$Al MAS NMR spectra of the remnant material obtained after selective dissolution under acidic conditions (process AD) show slight differences when compared to the spectrum of unreacted metakaolin, however the overall lineshape remains very similar. Higher intensity at $\delta_{obs}$ = 6 ppm is identified, indicating greater stability of Al(VI) species under acidic conditions when compared to Al(IV) and Al(V) species. The similarity between the residual solid phase after selective dissolution at neutral pH (process WD) and the as-cured geopolymers, and the similarity between the residual solid phase after selective dissolution under acidic conditions (process AD) and the metakaolin precursor, together indicate that the combined selective dissolution processes can quantify the amount of soluble, gel and insoluble content. Quantification of the gel and insoluble content will depend on the proportion of Al(IV), Al(V) and Al(VI) sites in the anhydrous metakaolin, and their relative stability under acidic conditions, however the effect on the quantified results will be minimal.

The $^{29}$Si MAS NMR spectra for the metakaolin precursor and geopolymer samples are shown in Figure 7. The spectra for each sample exhibit a broad resonance in a position typically attributed to

silicates and aluminosilicates [47]. Metakaolin exhibits a resonance centred at approximately $\delta_{iso}$= -103 ppm, consistent with that observed by Duxson et al. [8]. This position is associated with the presence of silicon in tetrahedral coordination ($Q^4$) and aluminium in a distribution of tetrahedral, pentahedral and octahedral coordination (as observed in $^{27}$Al MAS NMR analysis) in the silicate and aluminate layers of metakaolin[48]. Metakaolin comprises mainly $Q^4$(*m*Al) sites, as aluminosilicates which do not contain alkali or alkaline earth metals do not usually contain lower coordinated Si species (e.g. $Q^1$, $Q^2$ and $Q^3$) [8]. The position of this resonance suggests that it comprises primarily $Q^4$(1Al) silicon sites, however, spectral deconvolution shows a presence of other tetrahedral silicon sites, mainly $Q^4$(0Al) and $Q^4$(2Al).

After geopolymerisation, the main $^{29}$Si resonance shifts from $\delta_{iso}$ = -103 ppm in the metakaolin precursor to $\delta_{iso}$ = -84.8 ppm for Na[20](0.0), -86.1 ppm for Na[20](0.5), and -86.9 ppm for Na[20](1,0), indicating formation of Si sites within the M-A-S-H gel. The shifting of these resonances toward higher ppm is attributed to the replacement of Si by Al within the first coordination sphere of central Si atoms in the three-dimensional M-A-S-H gel framework [8,47]. The intensity and breadth of the main resonance is due to contributions from varying contents of overlapping $Q^4$(*m*Al) species, whose relative quantities can be determined from spectral deconvolution using Gaussian distributions. Figure 8 shows the $^{29}$Si NMR spectra and associated deconvolutions for each geopolymer sample and respective material after selective dissolution at neutral pH (process WD). The remnant unreactive metakaolin precursor (shaded spectra) is accounted for in the spectral deconvolutions by linearly scaling the intensity of anhydrous metakaolin precursor resonances (the relative intensity of which is determined from the relative amount of insoluble solid phase to gel content, converted from a mass basis to a molar basis, determined from the combined selective dissolution processes) as shown in Figure 2.

The $^{29}$Si spectral deconvolution for each sample comprises resonances at $\delta_{iso}$= -70, -85, -90, -95, -100, and -110 ppm. The resonance at approximately -70 ppm is attributed to $Q^0$ sites and is only observed in the samples with high silicate content (i.e. MS = 1.0). This resonance is therefore attributed to monomer silicate structures[49] from dissolved metakaolin and/or remnant soluble silicate that has

not reacted. For aluminosilicates and metakaolin-based geopolymers the peaks between $\delta_{iso}$ = -85 ppm and $\delta_{iso}$ = -110 ppm can be attributed to $Q^4(m\text{Al})$ sites, in agreement with other studies [8,47,50]. $Q^3$ and $Q^2$ sites resonate in the same region as $Q^4(m\text{Al})$ sites, making the coexistence of these species being possible, however the geopolymer framework has been shown to be fully polymerised and hence contains just $Q^4$ species[8,50]. This is consistent with $^{27}$Al MAS NMR data (presented above), which large amount of Al in tetrahedral coordination. Zeolite A contains $Q^4$(3Al) species [47] that resonate at -89.6 ppm in $^{29}$Si MAS NMR data, and hence will contribute to the intensity observed in this region in the $^{29}$Si MAS NMR data for samples containing this phase. As observed in the XRD data, halloysite is present in the metakaolin precursor and all geopolymer samples. Halloysite contains $Q^3$(1Al) sites that resonates at -93 ppm [51] and will therefore contribute to the intensity in this region of the $^{29}$Si MAS NMR data for all samples. Spectral deconvolution shows that in the systems with sodium silicate as part of the activator there is a greater formation of $Q^4$ sites with more Si within the second coordination sphere of the central Si atom. This is expected due to the high content of soluble silicates in the reaction mixture and correlates with the observed increase in compressive strength values for these samples (shown in Figure 1).

The amount of each $Q^4(m\text{Al})$ site in the spectral deconvolutions was quantified and is shown in Figure 9. Engelhardt's formula [52] (equation 1) was used to calculate the molar Si/Al ratio of the N-A-S-H gel from the normalised relative integral areas, $I_A$, of each resonance in the $^{29}$Si MAS NMR spectral deconvolutions from $Q^4(m\text{Al})$ sites in the NASH gel (excluding resonances due to $Q^4(m\text{Al})$ sites within remnant anhydrous metakaolin). Previous work has shown that Loewenstein's rule [53] (i.e. the absence of Al-O-Al bonds) is obeyed in synthetic alkali aluminosilicate gels with Si/Al > 1,[50] and is therefore assumed to be obeyed in the systems studied here.

$$\frac{\text{Si}}{\text{Al}} = \frac{\sum_{m=1}^{4} I_{AQ^4(m\text{Al})}}{\sum_{m=1}^{4} 0.25 \times m \times I_{AQ^4(m\text{Al})}} \quad \text{(equation 1)}$$

These results show that higher values of compressive strength in the geopolymers are associated with a higher gel Si/Al ratio (i.e. greater Si addition in the gel framework), which is in agreement with Duxson[8] and Fernandez-Jiménez [9]. This is readily observed in the Na[20](0.0) formulation, which

is the system with the lowest content of silica (i.e. lowest nominal Si/Al ratio). The Na[20](0.0) gel consists solely of $Q^4$(4Al) sites, and exhibits the lowest compressive strength of this series (when activator type and dose are held constant).

XRF analysis (Figure 5) showed the dissolution of a high percentage of $Na_2O$, $SiO_2$ and $Al_2O_3$ during selective dissolution at pH 7 (process WD). This change is also observed in the $^{29}Si$ and $^{27}Al$ MAS NMR data by the reduction in intensity of the broad resonances attributed to $Q^4$(4Al) sites and an increase in the intensity of resonances due to $Q^4$(3Al) sites and Si-rich sites $Q^4$(2Al) and $Q^4$(1Al). This increase in Si-rich sites is not due to the formation of new Si environments, but rather a relative increase to compensate the loss of $Q^4$(4Al) sites, consistent with the fact that Al-O-Si bonds are weaker than Si-O-Si bonds and will therefore dissolve preferentially. The system with a high content of soluble Si in the activator is less affected due to the lower amount of $Q^4$(4Al) sites within the gel framework.

To verify the effectiveness of the selective dissolution process, Figure 10 shows the $^{29}Si$ MAS NMR spectra for the remaining solid material obtained after selective dissolution in acidic conditions (process AD). In all systems, the broad resonance exhibits a position (centred between $\delta_{iso}$ = -103 ppm and -108 ppm) and line shape similar to that of metakaolin. A slight shift to lower ppm is observed for all analysed samples after selective dissolution in acidic conditions, and this is attributed to the slight preferential dissolution of Al(IV) species from the remnant unreacted metakaolin precursor. This results in slight reduction in the amount of $Q^4$(*m*Al) species with high *m* values and a slight increase in the amount of $Q^4$(*m*Al) species with low *m* values. This is consistent with the observations from $^{27}Al$ MAS NMR, XRD and XRF data discussed above, which together indicate that the combined selective dissolution processes can quantify the amount of soluble, gel and insoluble content. As discussed above, quantification of the gel and insoluble content will depend on the proportion of Al(IV), Al(V) and Al(VI) sites in the anhydrous metakaolin, and their relative stability under acidic conditions, however the effect on the quantified results will be minimal and is expected to be within the experimental errors inherent in the data used for this analysis.

3.5 FTIR analysis

The FTIR spectra for the anhydrous metakaolin precursor and the geopolymer system with an activator dosage of 20% $Na_2O$ are shown in Figure 11. In the spectrum for metakaolin, an intense peak is observed at approximately 1080 $cm^{-1}$ that according to Rees [32] is assigned to asymmetric stretching vibrations of Si-O-T bonds, where T= Si or Al in tetrahedral coordination. The band at approximately 800 $cm^{-1}$ is assigned to bending vibrations of Al-O bonds in $AlO_6$ octahedra [28]. Both of these bands are consistent with the $^{27}Al$ MAS NMR data for metakaolin discussed above. The geopolymerisation process is observed in the FTIR data by the shift of the main peak in each sample from 1080 $cm^{-1}$ to the region between 950 and 970 $cm^{-1}$. This change is due to the decrease in the Si/Al ratio[54] of the tetrahedral Si sites in the sample during geopolymer gel formation [28,55]. These were originally surrounded by low amounts of Al atoms (as much of the Al in metakaolin exists in Al(V) and Al(VI) sites). After dissolution of Al(VI) (indicated by the band at approximately 800 $cm^{-1}$and the $^{27}Al$ MAS NMR data discussed above), Al(V) and Al(IV) (indicated by the $^{27}Al$ MAS NMR data discussed above) from metakaolin during alkali-activation, the M-A-S-H gel framework is formed, with a larger number (relative to metakaolin) of Al atoms in tetrahedral coordination linked to tetrahedral Si atoms via oxygen bridges. This results in the observed shift of the band due to asymmetric stretching vibrations of Si-O-T bonds towards lower wavenumbers [56–58].

Comparing the different systems evaluated, the movement of the central bands to higher wavenumbers is observed in the systems with activators containing higher contents of soluble Si. This is associated with the higher quantity of Si in the Si-O-T bonds (i.e. higher gel Si/Al ratio). Previous works assigned signals in the range between 1020 $cm^{-1}$ and 998 $cm^{-1}$ to the asymmetric stretching vibrations of Si-O-T [11,28,54], and 940 $cm^{-1}$ and 979 $cm^{-1}$ to an asymmetric stretching vibration of non-bridging oxygen sites (Si-O-Na in the samples presented here)[11,28]. These two bands are identified in the spectra here by deconvolution of the main Si-O-T band. The use of sodium silicate as the alkali activator shifts the centre of this peak to higher wavenumber values. According to this, the addition of soluble silicate results in increased Si in the M-A-S-H gel structure, consistent with the $^{29}Si$ MAS NMR data discussed above, and a subsequent higher frequency Si-O-T vibration. The other

band observed close to 859 $cm^{-1}$ is attributed to bending of Si-OH bonds [11]. Bands at approximately 690 $cm^{-1}$ are the result of bending of Al-O-Si bonds [59], and indicate the formation of Al(IV) as the main Al environment in the geopolymer [28] (consistent with the $^{27}Al$ MAS NMR data discussed above).

According to Figure 11, the FTIR data for the solid material remaining after the selective dissolution process at neutral pH (process WD) exhibits a reduction in the intensity of the two main bands, which also shift to higher wavenumbers. This movement and change in intensity indicates the release of alkalis from Si-O-Na non-bridging oxygen sites (which result in the bands at approximately 940 $cm^{-1}$ and 979 $cm^{-1}$), as well as dissolution of a small amount of Al(IV) sites (observed via $^{27}Al$ and $^{29}Si$ MAS NMR above) which results in a reduction of Si-O-Al bonds. As observed in the $^{27}Al$ NMR results, aluminium is primarily present in tetrahedral coordination within the M-A-S-H gel structure, indicating the presence of a net negative charge due to $Al^{3+}$ substituting for $Si^{4+}$ that has been shown to be charge balanced by $Na^{+}$ ions in sodium silicate and sodium hydroxide activated metakaolin[8,11]. Previous work has shown that in the presence of sufficient quantities of Al the negative charge on tetrahedral Al in N-A-S-H gel systems can also be balanced by an extra-framework Al atom, coordinated by six framework oxygen atoms (i.e. Al(IV) species)[50]. Thus, the removal of alkalis induces the distortion of the aluminosilicate framework where the Si asymmetric stretching vibration (Si-O-T) is shifted to higher wavenumbers, which is also consistent with the reduction of Al(IV) environment. This was also observed by the reduction from the band intensity associated with Al(IV) in $^{27}Al$ MAS NMR analysis and can be associated with conversion of Al in tetrahedral to non-tetrahedral environments bonding to Si [28].

After selective dissolution under acidic conditions (process AD), the FTIR spectra for the residual materials are very similar to that of anhydrous metakaolin. The shift of the bands that were present in the FTIR spectra of the geopolymers to lower wavenumbers, and similar lineshape of the FTIR spectra of the solid material after selective dissolution under acidic conditions to that of anhydrous metakaolin demonstrates the efficacy of the combined selective dissolution process, consistent with the XRD and NMR results discussed above.

### 3.6 SEM analysis

Figure 12 shows the SEM secondary electron images of anhydrous metakaolin and the geopolymer system Na[20](1.0) before and after the selective dissolution under neutral pH (process WD) and acidic conditions (process AD). As expected, metakaolin (Figure 12A) comprises plate-shaped particles. For the geopolymer samples (which were ground and passed through a75 μm sieve prior to analysis) the particle size is larger than those of metakaolin. After selective dissolution at neutral pH (process WD), the particle size and shape remained the same as that of the geopolymer, indicating that the removal of the soluble elements did not cause a morphological change in the material. After selective dissolution under acidic conditions (process AD), the particle size is reduced when compared to the geopolymer and the original metakaolin. Some particles still remain plated-shaped, indicating a portion of unreacted material.

## 6. CONCLUSIONS

This study developed a selective dissolution process to systematically investigate the reaction extent of metakaolin-based geopolymers produced with different design parameters and curing conditions. The selective dissolution process, based on dissolution under neutral (pH 7) conditions to remove the water-soluble materials and dissolution under acidic conditions (pH 0) using a strong acid to remove the geopolymer gel, is an effective method and its efficacy is confirmed by a range of detailed spectroscopic and microstructural analyses. This approach provides a method for accurate quantification of soluble materials, gel content and insoluble materials within geopolymers.

The compressive strength is dictated by the gel nanostructure. The use of soluble silicate in the activator plays an important role in relation to the Si/Al ratio within the gel, observed via differing amounts of $Q^4(m\text{Al})$ sites. The Si/Al ratio of the geopolymer gel increases by the higher degree of reaction provided as a result of the addition of soluble silicate to the reaction mixture. Higher amounts of soluble silicate results in increased gel formation; however, this can results in an excess of alkali, due to reduced need for charge balancing of $Al^{3+}$ in tetrahedral sites, which is reflected in the large

amount of soluble alkali content. The compressive strength is also directly proportional to the amount of gel formed, although this effect is not as pronounced as that of the microstructural changes observed.

The content of soluble material in neutral pH conditions is mainly composed of $M_2O$, $SiO_2$ and $Al_2O_3$, where the alkalis are the main soluble fraction (representing values up to 50% of the total alkali content used) and the amount of alkali dissolution is dependent on the content of alkalis and soluble silicate of the activator. Spectroscopic and microstructural characterisation of the geopolymers shows that the extraction of alkalis from the geopolymer through a neutral dissolution process (water dissolution) results in a distortion of the framework structure with marked changes in the Al and Si environments. The removal of alkalis under neutral conditions shows nanostructural changes, including the reduction of $Q^4$(4Al) and Al(VI) species as observed by $^{29}$Si and $^{27}$Al MAS NMR and FTIR analysis. As the content of soluble silicate in the alkali activator is increased (i.e. higher MS content) the stability of Al-rich $Q^4$(*m*Al) sites is enhanced. This is visible in the system Na[20](1.0), with a high content of soluble silicate, which presents less nanostructural change when subjected to the dissolution process in a neutral environment.

Subsequent selective dissolution in acidic conditions dissolves the geopolymer gel content, leaving only the remnant unreacted metakaolin precursor which may then be quantified. Dissolution in acidic conditions also results in slight reduction in the amount of Al-rich $Q^4$(*m*Al) species from the remnant unreacted metakaolin precursor, and as such quantification of the gel and insoluble content will depend on the proportion of Al(IV), Al(V) and Al(VI) sites in the anhydrous metakaolin, and their relative stability under acidic conditions. The effect on the quantified results will, however, be minimal and is expected to be within the experimental errors inherent in the data used for this type of analysis.

The combined selective dissolution process provided here can therefore quantify the amount of soluble material, geopolymer gel and unreacted precursor in Ca-free geopolymer systems. This provides valuable new insight into the reaction product formed in metakaolin-based geopolymers, the

state of alkalis in the structure and the nature of the selective dissolution processes, knowledge that is essential to define the design parameters and predict the durability of geopolymers materials.

ACKNOWLEDGEMENTS

Funding from Australian Research Council through a Discovery project and a DECRA DE/170/101070 project. M.A. Longhi is grateful for the financial support of CAPES and of SWE 203750/2017-9. The participation of Brazilian authors was sponsored by CNPq (Brazilian National Council for Scientific and Technological Development) through the research project UNIVERSAL grant number 458597/2014-7, as well as the research fellowships PQ2017 303753/2017-0 and 305530/2017-8. The participation of B. Walkley was supported by the Engineering and Physical Sciences Research Council (UK) through grant EP/P013171/1. The authors wish to thank and acknowledge Professor John L. Provis, The University of Sheffield, for very insightful discussions related to this work. The authors also wish to thank and acknowledge Dr Sandra van Meurs, Department of Chemistry, The University of Sheffield, for assistance in acquiring the NMR data and insightful discussions related to this work.

**REFERENCES:**


[1] Van Deventer JSJ, Provis JL, Duxson P. Technical and commercial progress in the adoption of geopolymer cement. Miner Eng 2011;29:89–104. doi:10.1016/j.mineng.2011.09.009.

[2] Provis JL, Bernal S a. Geopolymers and Related Alkali-Activated Materials. Annu Rev Mater Res 2014;44:299–327. doi:10.1146/annurev-matsci-070813-113515.

[3] Bernal SA, Rodríguez ED, Kirchheim AP, Provis JL. Management and valorisation of wastes through use in producing alkali-activated cement materials. J Chem Technol Biotechnol 2016. doi:10.1002/4927.

[4] McLellan BC, Williams RP, Lay J, van Riessen A, Corder GD. Costs and carbon emissions for geopolymer pastes in comparison to ordinary portland cement. J Clean Prod 2011;19:1080–90.

[5] Heath A, Paine K, McManus M. Minimising the global warming potential of clay based geopolymers. J Clean Prod 2014;78:75–83. doi:10.1016/j.jclepro.2014.04.046.

[6] Habert G, Ouellet-plamondon C. Recent update on the environmental impact of geopolymers Rilem Technical Leters 2016; 1:17–23.

[7] Provis JL, Lukey GC, van Deventer JSJ. Do Geopolymers Actually Contain Nanocrystalline Zeolites: A Reexamination of Existing Results. Chem Mater 2005;17:3075–85. doi:10.1021/cm050230i.

[8] Duxson P, Provis JL, Lukey GC, Separovic F, Deventer JSJ Van. Si NMR Study of Structural Ordering in Aluminosilicate Geopolymer Gels. Langmuir 2005:3028–36. doi:10.1021/la047336x.

[9] Fernández-Jiménez A, Palomo A, Sobrados I, Sanz J. The role played by the reactive alumina content in the alkaline activation of fly ashes. Microporous and Mesoporous Materials 2006;91:111–9. doi:10.1016/j.micromeso.2005.11.015.

[10] Oelkers EH, Gislason SR. The mechanism, rates and consequences of basaltic glass dissolution: I. An experimental study of the dissolution rates of basaltic glass as a function of aqueous Al, Si and oxalic acid concentration at 25°C and pH = 3 and 11. Geochim Cosmochim Acta 2001;65:3671–81. doi:10.1016/S0016-7037(01)00664-0.

[11] Zhang Z, Provis JL, Wang H, Bullen F, Reid A. Quantitative kinetic and structural analysis of geopolymers. Part 2. Thermodynamics of sodium silicate activation of metakaolin. Thermochim Acta 2013;565:163–71. doi:10.1016/j.tca.2013.01.040.

[12] Zhang Z, Provis JL, Reid A, Wang H. Fly ash-based geopolymers : The relationship between composition , pore structure and efflorescence. Cement and Concrete Research 2014;64:30–41.

[13] Yao X, Yang T, Zhang Z. Compressive strength development and shrinkage of alkali-activated fly ash–slag blends associated with efflorescence. Mater Struct Constr 2016;49:2907–18. doi:10.1617/s11527-015-0694-3.

[14] Zhang Z, Provis JL, Ma X, Reid A, Wang H. Efflorescence and subflorescence induced microstructural and mechanical evolution in fly ash-based geopolymers. Cem Concr Compos 2018;92:165–77. doi:10.1016/j.cemconcomp.2018.06.010.

[15] Duxson P, Lukey GC, Separovic F, van Deventer JSJ. Effect of alkali cations on aluminum incorporation in geopolymeric gels. Ind Eng Chem Res 2005;44:832–9. doi:10.1021/ie0494216.

[16] Rowles, Matthew R. Hanna, J. V. Pike, K. J, smith, M. E o'connor BH. Si, Al, 1 H and 23 Na MAS NMR Study of the Bonding Character in Aluminosilicate Inorganic Polymers 27. Appl Magentic Reson 2007;32:663–89. doi:10.1007/s00723-007-0043-y.

[17] Najafi E, Allahverdi A, Provis JL. Efflorescence control in geopolymer binders based on natural pozzolan. Cement & Concrete Composites 2012;34:25–33.

doi:10.1016/j.cemconcomp.2011.07.007.

[18] Zhang Z, Provis JL, Reid A, Wang H. Fly ash-based geopolymers: The relationship between composition, pore structure and efflorescence. Cem Concr Res 2014;64:30–41. doi:10.1016/j.cemconres.2014.06.004.

[19] Škvára F, Šmilauer V, Hlaváček P, Kopecký L, Cílová Z. A weak alkali bond in (N, K)-A-S-H gels: Evidence from leaching and modeling. Ceram - Silikaty 2012;56:374–82.

[20] Lloyd RR, Provis JL, Van Deventer JSJ. Pore solution composition and alkali diffusion in inorganic polymer cement. Cem Concr Res 2010;40:1386–92. doi:10.1016/j.cemconres.2010.04.008.

[21] Zhang Z, Provis JL, Zou J, Reid A, Wang H. Toward an indexing approach to evaluate fly ashes for geopolymer manufacture. Cem Concr Res 2016;85:163–73. doi:10.1016/J.CEMCONRES.2016.04.007.

[22] Williams RP, Hart RD, Riessen A Van. Quantification of the Extent of Reaction of Metakaolin-Based Geopolymers Using X-Ray Diffraction, Scanning Electron Microscopy, and Energy-Dispersive Spectroscopy J Am Ceram Soc 2011;2670:2663–70. doi:10.1111/j.1551-2916.2011.04410.x.

[23] Chen-Tan NW, van Riessen A, Ly C V, Southam DC. Determining the Reactivity of a Fly Ash for Production of Geopolymer. J Am Ceram Soc 2009;887:881–7. doi:10.1111/j.1551-2916.2009.02948.x.

[24] Li Y, Lin H, Wang Z. Quantitative analysis of fly ash in hardened cement paste. Constr Build Mater 2017;153:139–45. doi:https://doi.org/10.1016/j.conbuildmat.2017.07.106.

[25] Gao X, Yu QL, Brouwers HJH. Apply 29Si, 27Al MAS NMR and selective dissolution in identifying the reaction degree of alkali activated slag-fly ash composites. Ceram Int 2017;43:12408–19. doi:https://doi.org/10.1016/j.ceramint.2017.06.108.

[26] Dyson HM, Richardson IG, Brough AR, Bogue T. A Combined 29 Si MAS NMR and Selective Dissolution Technique for the Quantitative Evaluation of Hydrated Blast Furnace Slag. Cement Blends 2007;602:598–602. doi:10.1111/j.1551-2916.2006.01431.x.

[27] Lumley JS, Gollop RS, Moir GK. Degrees of reation of the slag in some blends with Portland cement. Cem Concr Res 1996;26:139–51.

[28] Zhang Z, Wang H, Provis JL, Bullen F, Reid A, Zhu Y. Quantitative kinetic and structural analysis of geopolymers. Part 1. The activation of metakaolin with sodium hydroxide. Thermochim Acta 2012;539:23–33. doi:10.1016/j.tca.2012.03.021.

[29] Longhi MA, Rodríguez ED, Bernal SA, Provis JL, Kirchheim AP. Valorisation of a kaolin mining waste for the production of geopolymers. J Clean Prod 2016; 115: 265-272.

[30] Massiot D, Fayon F, Capron M, King I, Le Calvé S, Alonso B, et al. Modelling one- and two-dimensional solid-state NMR spectra. Magn Reson Chem 2001;40:70–6. doi:10.1002/mrc.984.

[31] Provis JL, Duxson P, Lukey GC, van Deventer JSJ. Statistical Thermodynamic Model for Si/Al Ordering in Amorphous Aluminosilicates. Chem Mater 2005;17:2976–86. doi:10.1021/cm050219i.

[32] Rees CA, Provis JL, Lukey GC, van Deventer JSJ. In Situ ATR-FTIR Study of the Early Stages of Fly Ash Geopolymer Gel Formation. Langmuir 2007;23:9076–82. doi:10.1021/la701185g.

[33] Wan Q, Rao F, Song S, García RE, Estrella RM, Patiño CL, et al. Geopolymerization reaction, microstructure and simulation of metakaolin-based geopolymers at extended Si/Al ratios. Cem Concr Compos 2017;79:45–52. doi:10.1016/j.cemconcomp.2017.01.014.

[34] Gao K, Lin K-L, Wang D, Hwang C-L, Shiu H-S, Chang Y-M, et al. Effects SiO2/Na2O molar ratio on mechanical properties and the microstructure of nano-SiO2 metakaolin-based geopolymers. Constr Build Mater 2014;53:503–10. doi:10.1016/j.conbuildmat.2013.12.003.

[35] Dimas D, Giannopoulou I, Panias D. Polymerization in sodium silicate solutions: A fundamental process in geopolymerization technology. J Mater Sci 2009;44:3719–30. doi:10.1007/s10853-009-3497-5.

[36] Giannopoulou I, Panias D. Hydrolytic stability of sodium silicate gels in the presence of aluminum. J Mater Sci 2010;45:5370–7. doi:10.1007/s10853-010-4586-1.

[37] Duxson P, Mallicoat SW, Lukey GC, Kriven WM, van Deventer JSJ. The effect of alkali and Si/Al ratio on the development of mechanical properties of metakaolin-based geopolymers. Colloids Surfaces A Physicochem Eng Asp 2007;292:8–20. doi:10.1016/j.colsurfa.2006.05.044.

[38] Yamamoto S, Sugiyama S, Matsuoka O, Kohmura K. Dissolution of Zeolite in Acidic and Alkaline Aqueous Solutions As Revealed by AFM Imaging 1996;3654:18474–82.

[39] Hartman RL, Fogler HS, Arbor A. Understanding the Dissolution of Zeolites. Langmuir 2007:5477–84.

[40] Duxson P, Fernández-Jiménez a., Provis JL, Lukey GC, Palomo a., Deventer JSJ. Geopolymer technology: the current state of the art. J Mater Sci 2006;42:2917–33. doi:10.1007/s10853-006-0637-z.

[41] Smith ME, Neal G, Trigg MB, Drennan J. Structural characterization of the thermal transformation of halloysite by solid state NMR. Appl Magn Reson 1993;4:157–70. doi:10.1007/BF03162561.

[42] Newman RH, Childs CW, Churchman GJ. Aluminium coordination and structural disorder in halloysite and kaolinite by 27Al NMR spectroscopy. Clay Miner 1994;29:305–12. doi:DOI: 10.1180/claymin.1994.029.3.01.

[43] MacKenzie KJD, Brew DRM, Fletcher RA, Vagana R. Formation of aluminosilicate geopolymers from 1:1 layer-lattice minerals pre-treated by various methods: a comparative study. J Mater Sci 2007;42:4667–74. doi:10.1007/s10853-006-0173-x.

[44] Walkley B, San Nicolas R, Sani M-A, Gehman JD, van Deventer JSJ, Provis JL. Phase evolution of $Na_2O$–$Al_2O_3$–$SiO_2$–$H_2O$ gels in synthetic aluminosilicate binders. Dalt Trans 2016;45:5521–35. doi:10.1039/C5DT04878H.

[45] Lippmaa E, Samoson A, Magi M. High-resolution aluminum-27 NMR of aluminosilicates. J Am Chem Soc 1986;108:1730–5. doi:10.1021/ja00268a002.

[46] Yang H, Walton RI, Antonijevic S, Wimperis S, Hannon AC, Facility I. Local Order of Amorphous Zeolite Precursors from 29 Si {1 H} CPMAS and 27 Al and 23 Na MQMAS NMR and Evidence for the Nature of Medium-Range Order from Neutron Diffraction 2004:8208–17. doi:10.1021/jp037887g.

[47] Engelhardt G, Michel D. High-resolution solid-state NMR of silicates and zeolites. vol. 499 p. John Wiley and Sons, New York, NY; 1987.

[48] White CE, Provis JL, Proffen T, Riley DP, van Deventer JSJ. Density Functional Modeling of the Local Structure of Kaolinite Subjected to Thermal Dehydroxylation. J Phys Chem A 2010;114:4988–96. doi:10.1021/jp911108d.

[49] Bass JL, Turner GL. Anion distributions in sodium silicate solutions. Characterization by 29Si NMR and infrared cpectroscopies, and vapor phase osmometry. J Phys Chem B 1997;101:10638–44. doi:10.1021/jp9715282.

[50] Walkley B, Rees GJ, Nicolas RS, Deventer JSJ Van, Hanna J V, Provis JL. New Structural Model of Hydrous Sodium Aluminosilicate Gels and the Role of Charge-Balancing Extra-Framework Al. J. Phys. Chem. 2018;4. doi:10.1021/acs.jpcc.8b00259.

[51] Cervini-Silva J, Nieto-Camacho A, Palacios E, Montoya JA, Gómez-Vidales V, Ramírez-Apán MT. Anti-inflammatory and anti-bacterial activity, and CYTOTOXICITY of halloysite surfaces. Colloids Surfaces B Biointerfaces 2013;111:651–5.

doi:https://doi.org/10.1016/j.colsurfb.2013.06.056.

[52] Engelhardt G, Lohse U, Lippmaa E, Tarmak M, Mägi M. 29Si-NMR-Untersuchungen zur Verteilung der Silicium-und Aluminiumatome im Alumosilicatgitter von Zeolithen mit Faujasit-Struktur. ZAAC - J Inorg Gen Chem 1981;482:49–64. doi:10.1002/zaac.19814821106.

[53] Loewenstein W. The distribution of aluminum in the tetrahedra of silicates and aluminates. Am Mineral 1954;39:92–6.

[54] Criado M, Palomo A, Fernandez-Jimenez A. Alkali activation of fly ashes . Part 1 : Effect of curing conditions on the carbonation of the reaction products. Fuel 2005;84:2048–54. doi:10.1016/j.fuel.2005.03.030.

[55] Granizo N, Palomo A, Fernandez-Jimenez A. Effect of temperature and alkaline concentration on metakaolin leaching kinetics. Ceram Int 2014;40:8975–85. doi:10.1016/j.ceramint.2014.02.071.

[56] Hajimohammadi A, Provis JL, van Deventer JSJ. The effect of silica availability on the mechanism of geopolymerisation. Cem Concr Res 2011;41:210–6. doi:10.1016/j.cemconres.2011.02.001.

[57] Lee WKW, van Deventer JSJ. Effects of anions on the formation of aluminosilicate gel in geopolymers. Ind Eng Chem Res 2002;41:4550–8. doi:doi:10.1021/ie0109410.

[58] Rees CA, Provis JL, Lukey GC, Deventer JSJ Van. Attenuated Total Reflectance Fourier Transform Infrared Analysis of Fly Ash Geopolymer Gel Aging. Langmuir 2007:8170–9.

[59] Bernal S a., Provis JL, Rose V, Mejía de Gutierrez R. Evolution of binder structure in sodium silicate-activated slag-metakaolin blends. Cem Concr Compos 2011;33:46–54. doi:10.1016/j.cemconcomp.2010.09.004.

[60] Engelhardt G. Multinuclear solid-state NMR in silicate and zeolite chemistry. Trend in analytical chemistry 1989;8:343–7.

Table 1 – Chemical composition and particle size of metakaolin

| | | |
|---|---|---|
| Particle size (μm) | $d_{10}$ | 0.82 |
| | $d_{50}$ | 3.52 |
| | $d_{90}$ | 10.04 |
| | Median particle size | 4.56 |
| Composition | Oxide | Wt. % |
| | $SiO_2$ | 54.82 |
| | $Al_2O_3$ | 42.47 |
| | $TiO_2$ | 1.23 |
| | $Fe_2O_3$ | 0.48 |
| | $Na_2O$ | 0.35 |
| | $K_2O$ | 0.17 |
| | CaO | 0.17 |
| | $SO_3$ | 0.11 |
| | $P_2O_5$ | 0.09 |
| | L.O.I (loss of ignition at 950°C) | 0.11 |

Table 2 - Formulation of geopolymer samples

| Geopolymers | MK | NaOH or KOH | SS | $H_2O$ |
|---|---|---|---|---|
| Na [25](1.0) | 100 | 16.6 | 82.3 | 42.2 |
| Na [25](0.5) | 100 | 24.5 | 41.1 | 64.7 |
| Na [25](0.0) | 100 | 32.3 | 0.0 | 79.4 |
| Na [20](1.0) | 100 | 13.3 | 65.8 | 44.8 |
| Na [20](0.5) | 100 | 19.6 | 32.9 | 63.7 |
| Na [20](0.0) | 100 | 25.8 | 0.0 | 75.5 |
| Na[15](1.0) | 100 | 10.0 | 49.4 | 54.0 |
| Na [15](0.5) | 100 | 14.7 | 24.7 | 62.8 |
| Na [15](0.0) | 100 | 19.4 | 0.0 | 71.6 |
| Na+K [20](1.0) | 100 | 15.6 | 46.2 | 51.2 |
| Na+K [20](0.5) | 100 | 20.0 | 21.3 | 66.9 |
| Na+K [20](0.0) | 100 | 23.8 | 0.0 | 74.3 |
| Na 50° [20](1.0) | 100 | 13.3 | 65.8 | 44.8 |
| Na 50° [20](0.5) | 100 | 19.6 | 32.9 | 63.7 |
| Na 50° [20](0.0) | 100 | 25.8 | 0.0 | 75.5 |

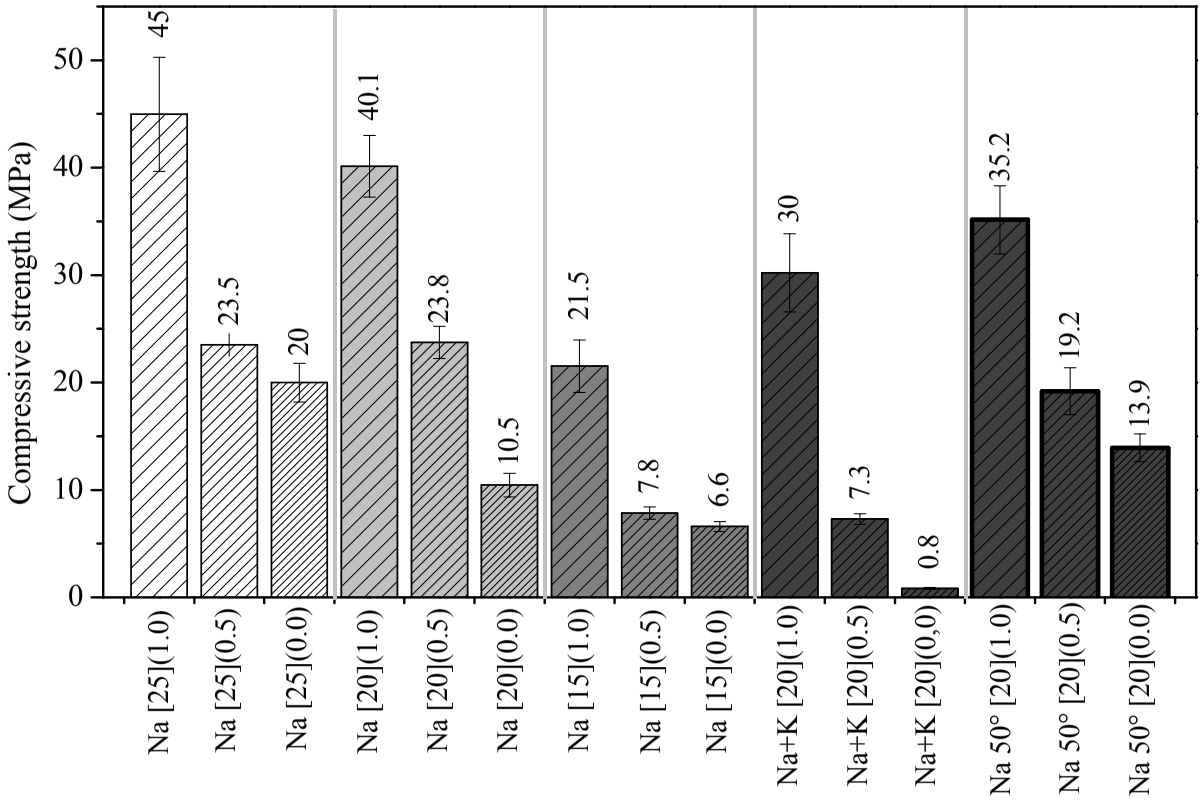


Figure 1– Compressive strength values for geopolymers cured for 28 days

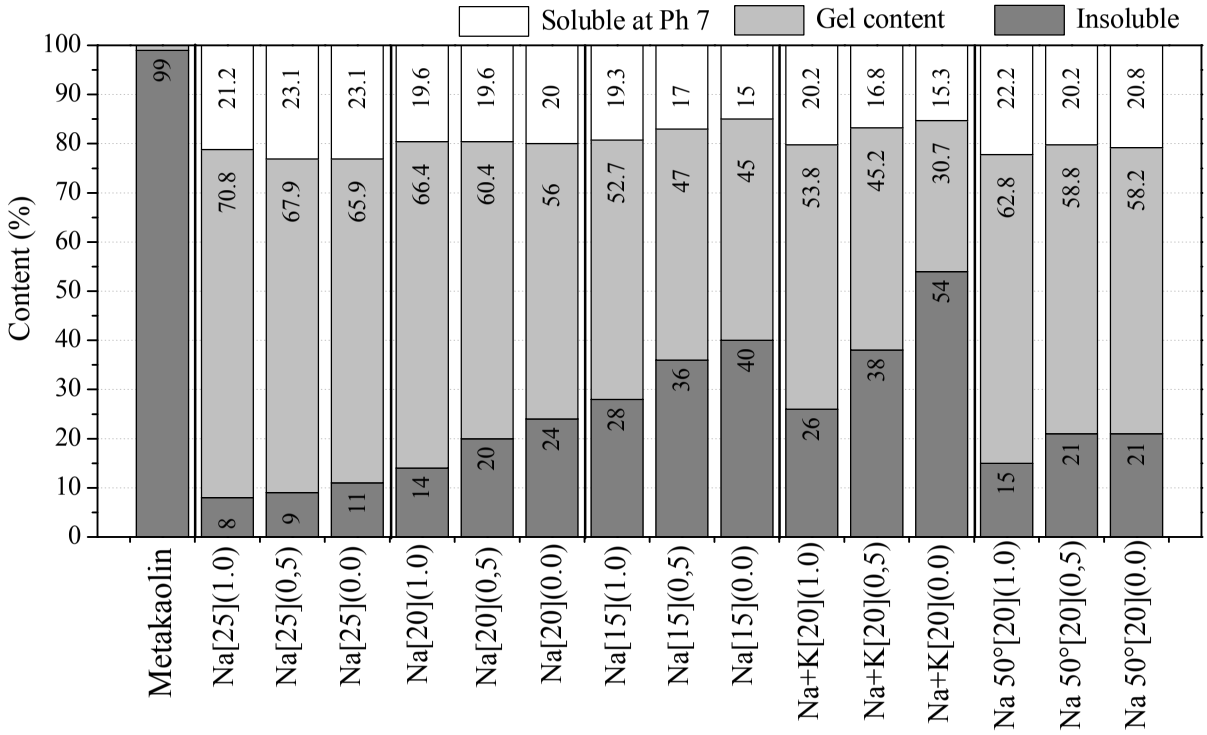


Figure 2 – Relative content of soluble, insoluble and gel material in metakaolin-based geopolymers determined from water dissolution and acid dissolution

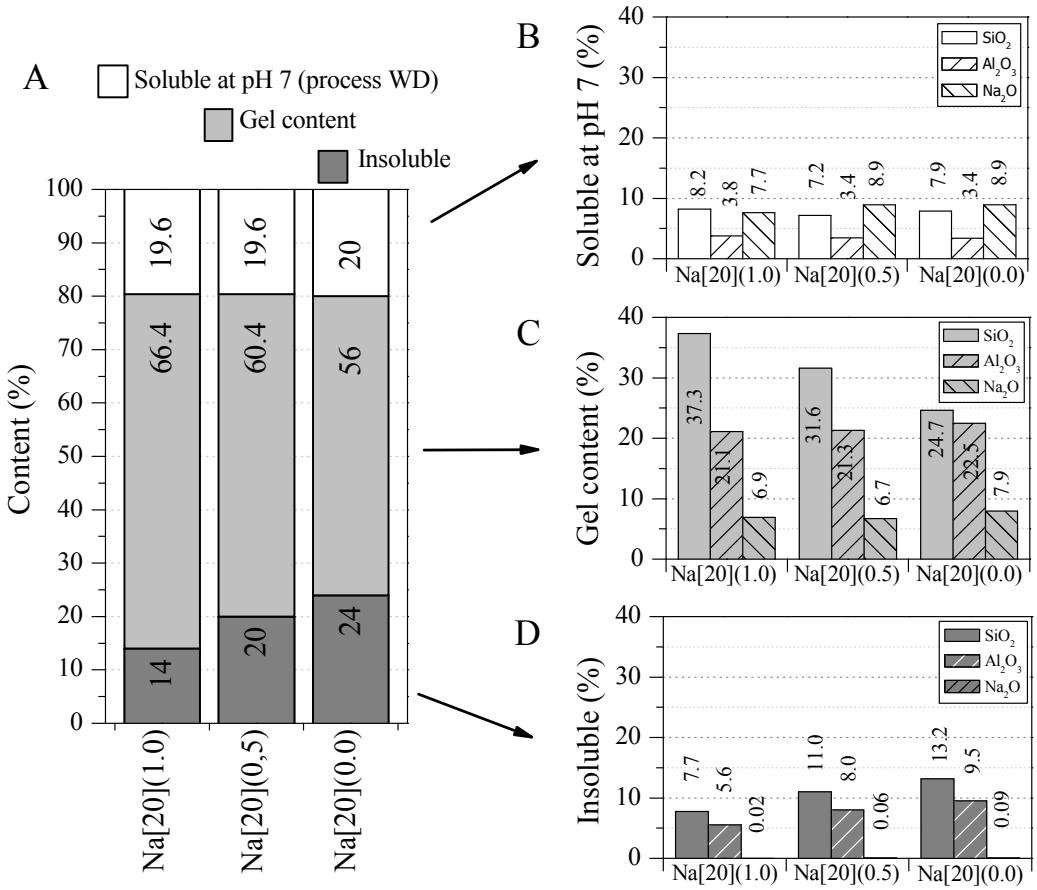


Figure 3 – Oxide compositions ($SiO_2$, $Al_2O_3$ and $Na_2O$, mass basis, as a percentage of either the soluble at pH 7, gel or insoluble content as shown in A, B and C) of the solid phase obtained after the selective dissolution processes. A: The fraction of soluble, gel and insoluble components in geopolymers with Na[20]. B: Oxide compositions in the soluble content (obtained from process WD) (calculated from the gel, insoluble and total content). C: Oxide compositions in the gel content (obtained from process AD). D: oxide compositions in the insoluble content (obtained from process AD). All values are normalised such that the total sample material is 100 wt.%.

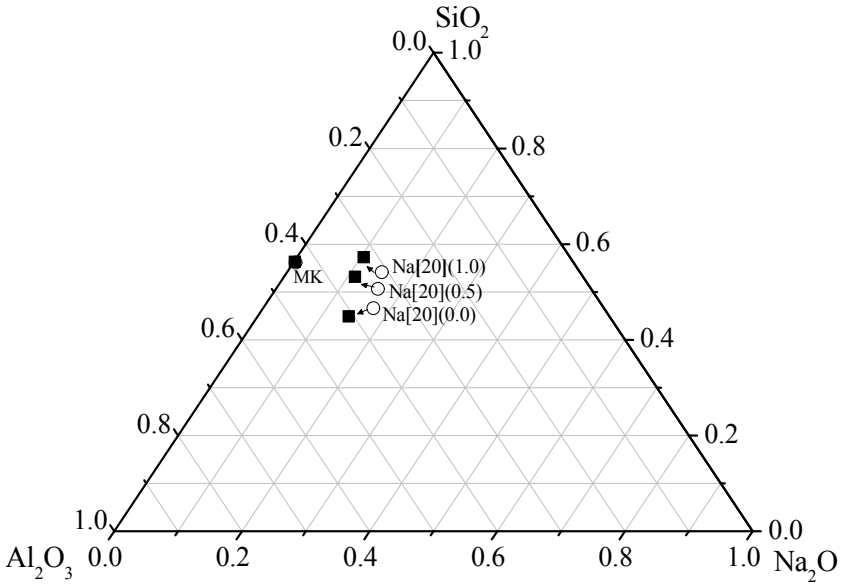


Figure 4 - Ternary diagram showing the chemical composition of the initial geopolymer formulation (white circles) and geopolymer gel formed (black squares) in the $SiO_2$-$Al_2O_3$-$Na_2O$ system.

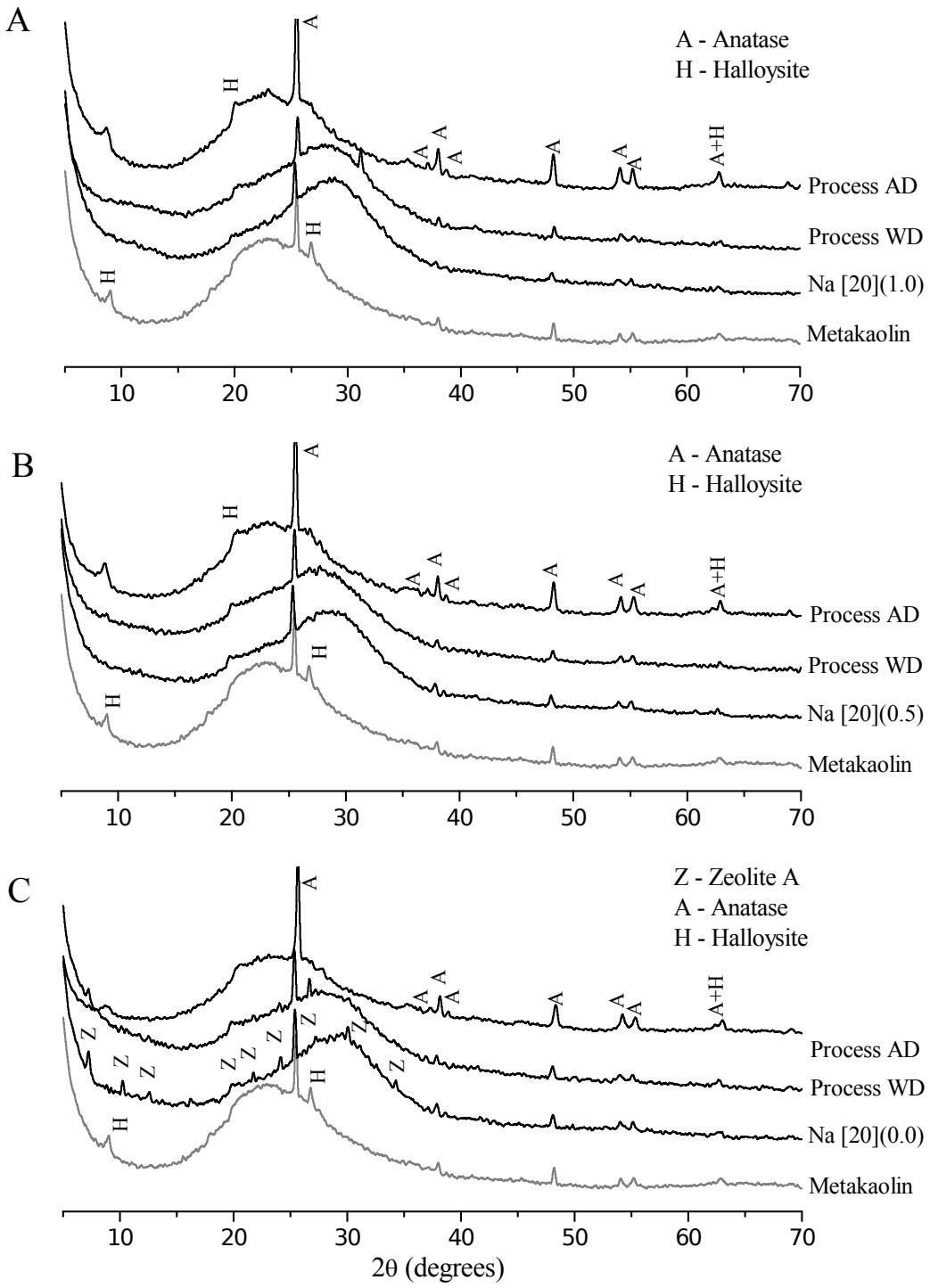


Figure 5 – XRD patterns of the anhydrous metakaolin precursor and geopolymers before and after the selective dissolution processes WD and AD. A: Na[20](1.0), B:Na[20](0.5), C: Na[20](0.0).

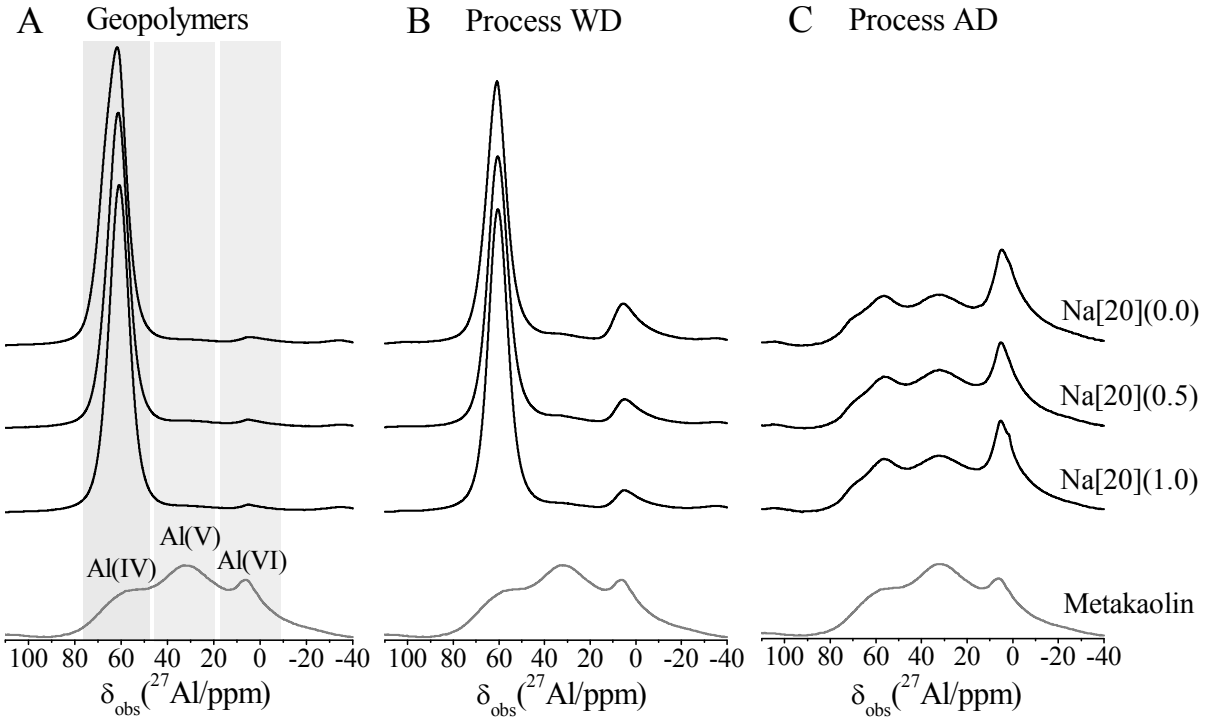


Figure 6 - $^{27}Al$ MAS NMR spectra (11.7 T, $\nu_R$ = 12.5 kHz) of the metakaolin precursor and geopolymers samples after selective dissolution under neutral pH (process WD) and acidic conditions (process AD). A: anhydrous metakaolin and geopolymers, B: after selective dissolution under neutral pH (process WD), C: selective dissolution under acidic conditions (process AD).

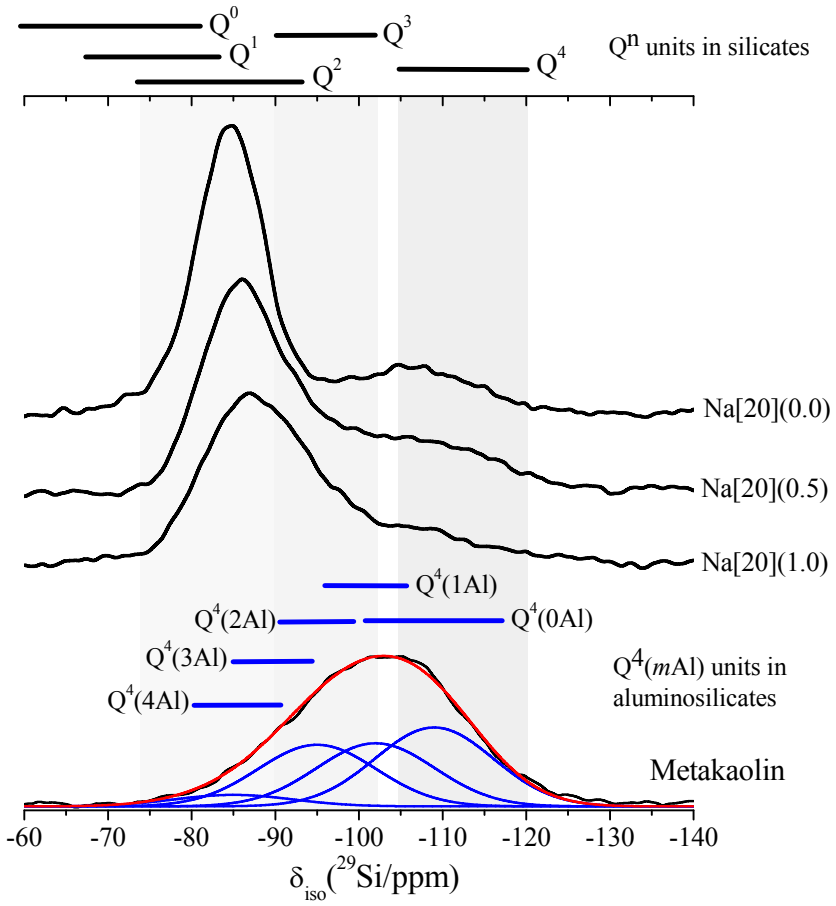


Figure 7 - $^{29}$Si MAS NMR (11.7 T, $\nu_R$ = 12.5 kHz) data (black lines) of the anhydrous metakaolin precursor and geopolymers. Q$^4$(*m*Al) assignments are made with reference to the scientific literature as noted in the main text and summarised by Engelhardt et al.[60]. The simulation (red line) of the $^{29}$Si MAS NMR spectra for anhydrous metakaolin precursor and associated spectral devonvolutions (blue lines) are shown at the bottom of the figure.

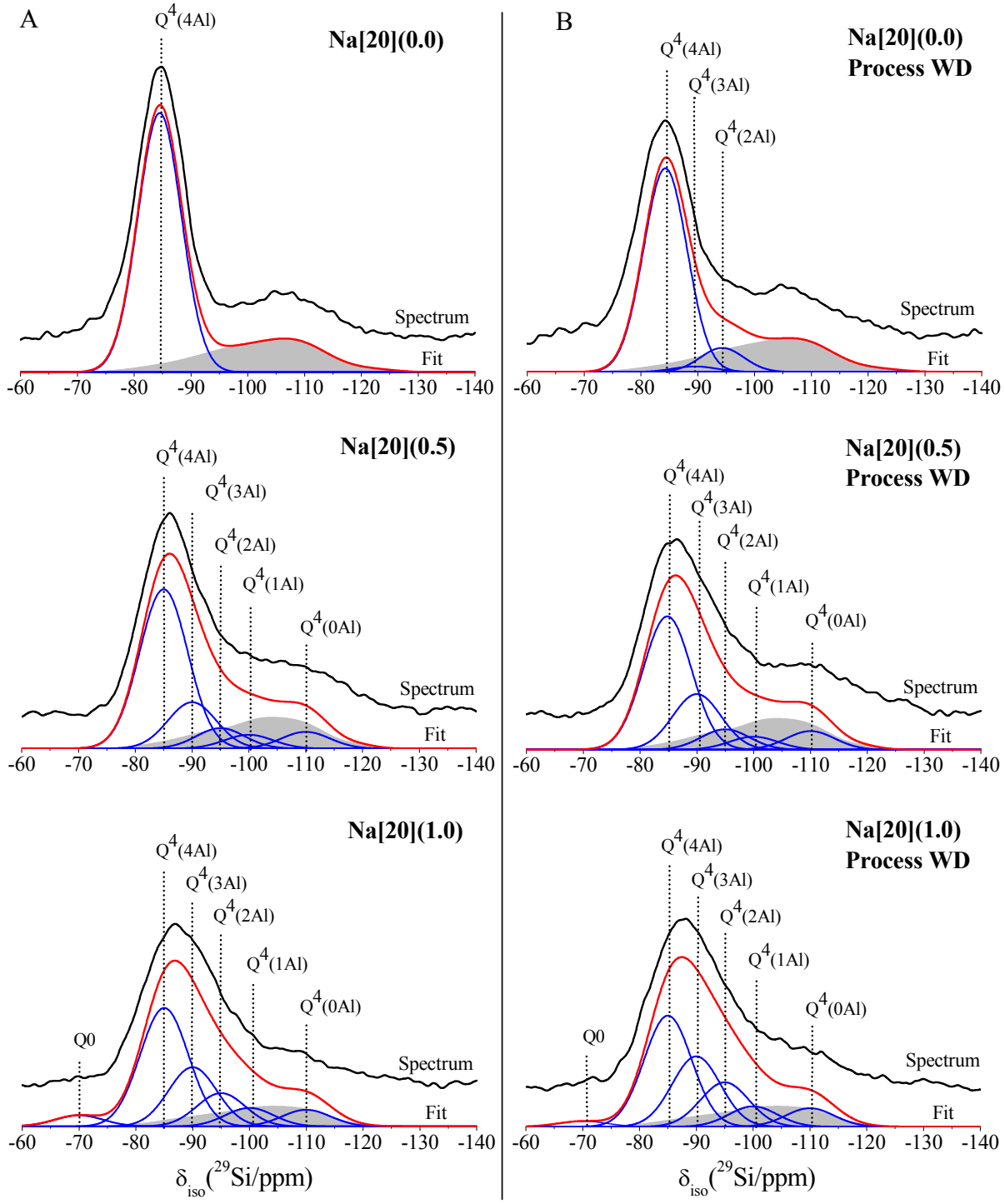


Figure 8 – $^{29}$Si MAS NMR (11.7 T, $\nu_R$ = 12.5 kHz) data (black lines), simulations (red lines) and spectral deconvolutions (blue lines) for each geopolymer sample before and after selective dissolution at neutral pH (process WD). A: Deconvolution of spectra for the geopolymers and B: deconvolution of spectra for the solid phase obtained after the dissolution process WD. $Q^4(m\text{Al})$ assignments are made with reference to the scientific literature as noted in the main text and summarised by Engelhardt et al.[47]. The contribution from remnant unreacted metakaolin is shown as the shaded grey area.

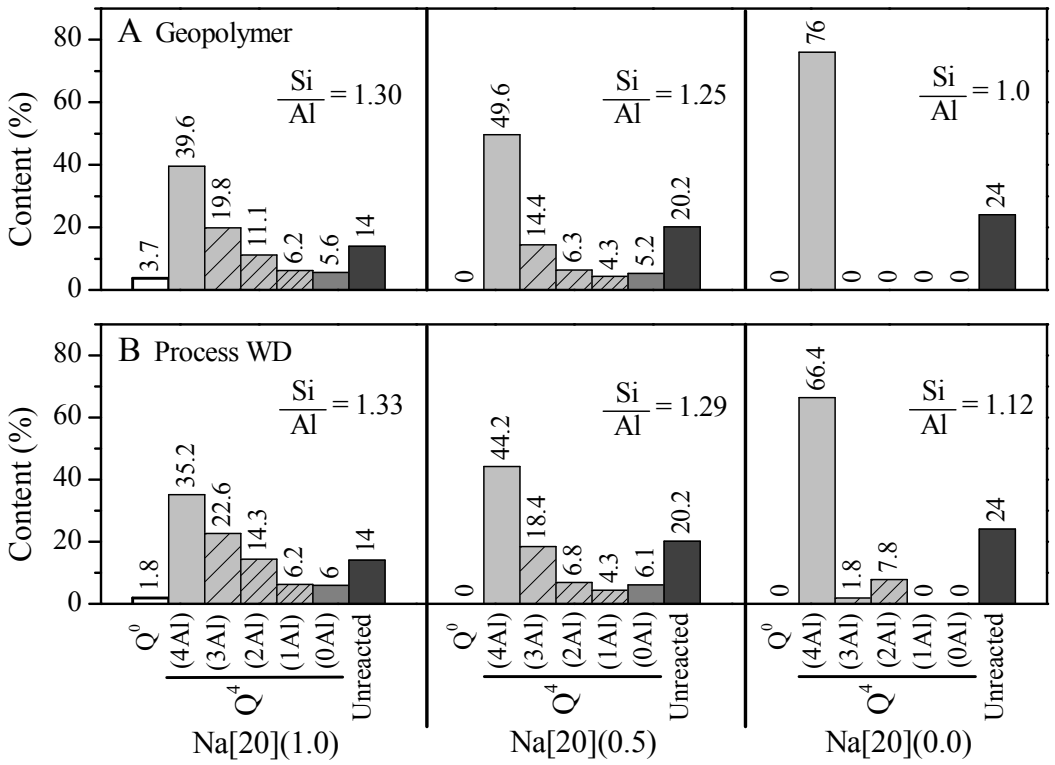


Figure 9 – $^{29}$Si MAS NMR (11.7 T, $\nu_R$ = 12.5 kHz) peak quantification for each geopolymer sample before and after the selective dissolution at neutral pH (process WD)

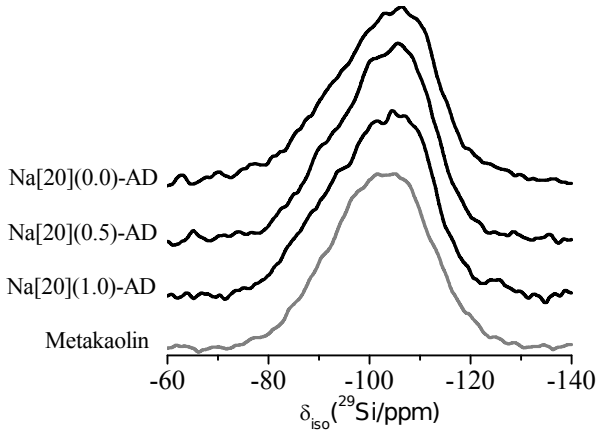


Figure 10 – $^{29}$Si MAS NMR spectra (11.7 T, $\nu_R$ = 12.5 kHz) of unreacted metakaolin and geopolymer samples after selective dissolution under acidic conditions (process AD).

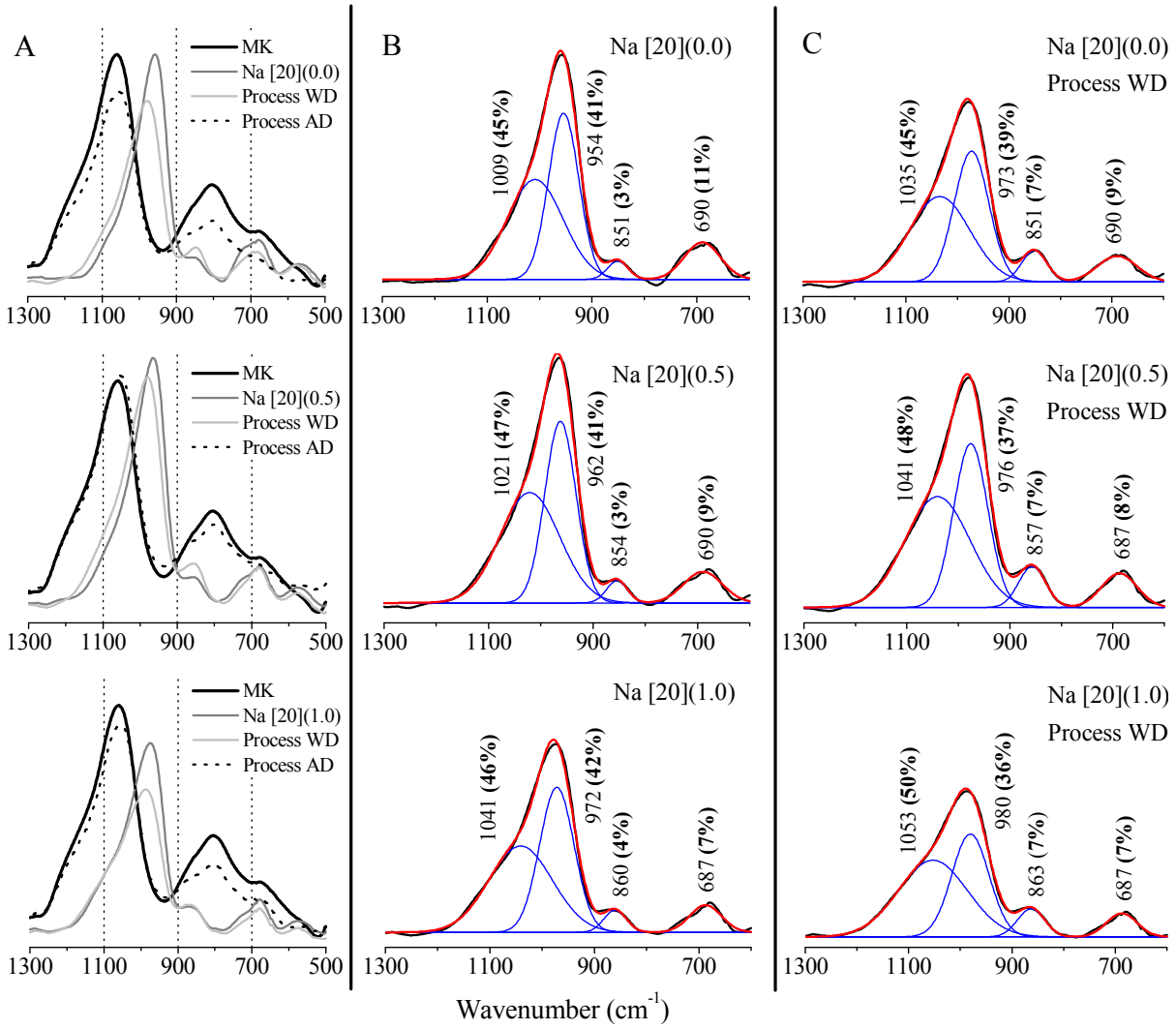


Figure 11 - FTIR spectra (absorbance) for the metakaolin precursor and geopolymer systems with an activator dose of 20% $Na_2O$ before and after each dissolution process. A: The anhydrous metakaolin, geopolymer and solid material obtained after the dissolution processes WD and AD, B: Deconvolution of spectra for the geopolymers and C: deconvolution of spectra for the solid material obtained after selective dissolution at neutral pH (process WD).

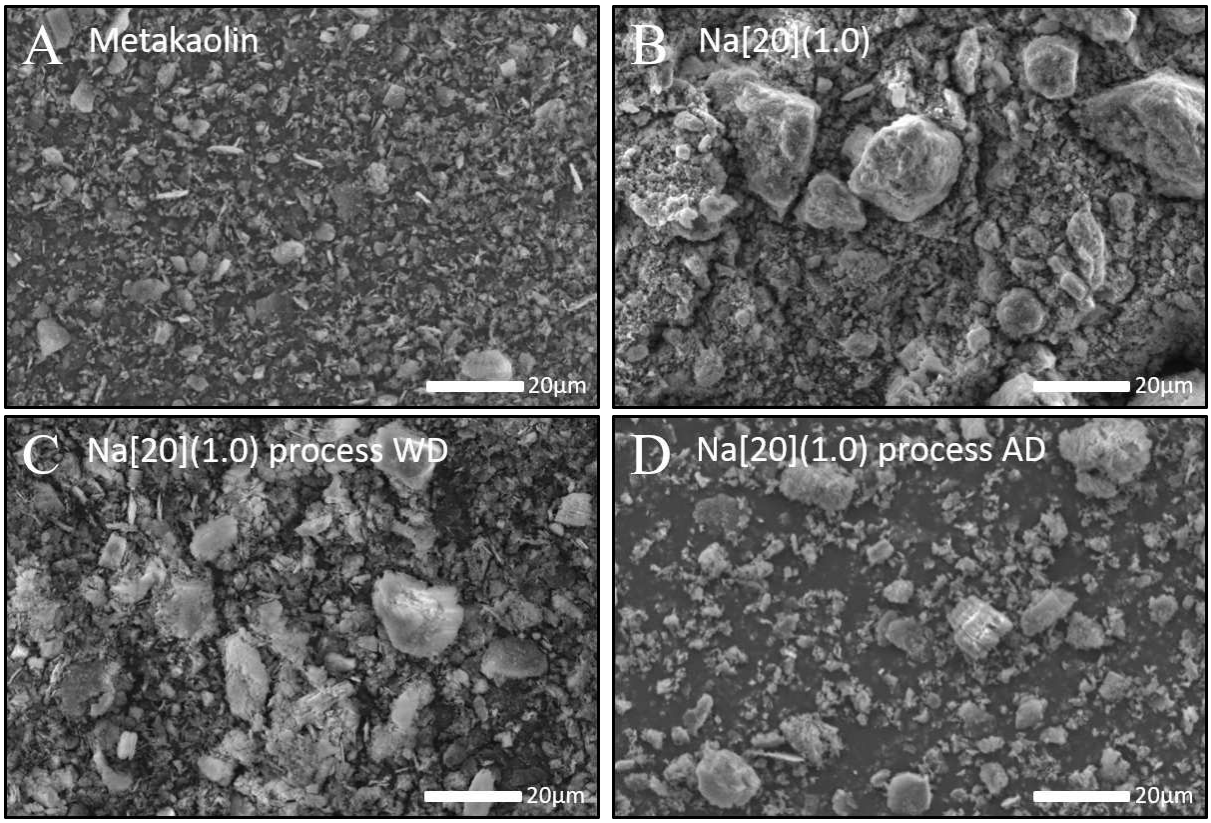

Figure 12 - SEM secondary electron images of A: anhydrous metakaolin, B: geopolymer Na [20](1.0), C: Na [20](1.0) after selective dissolution at neutral pH (process WD) and D: Na [20](1.0) after selective dissolution under acidic conditions (process AD).

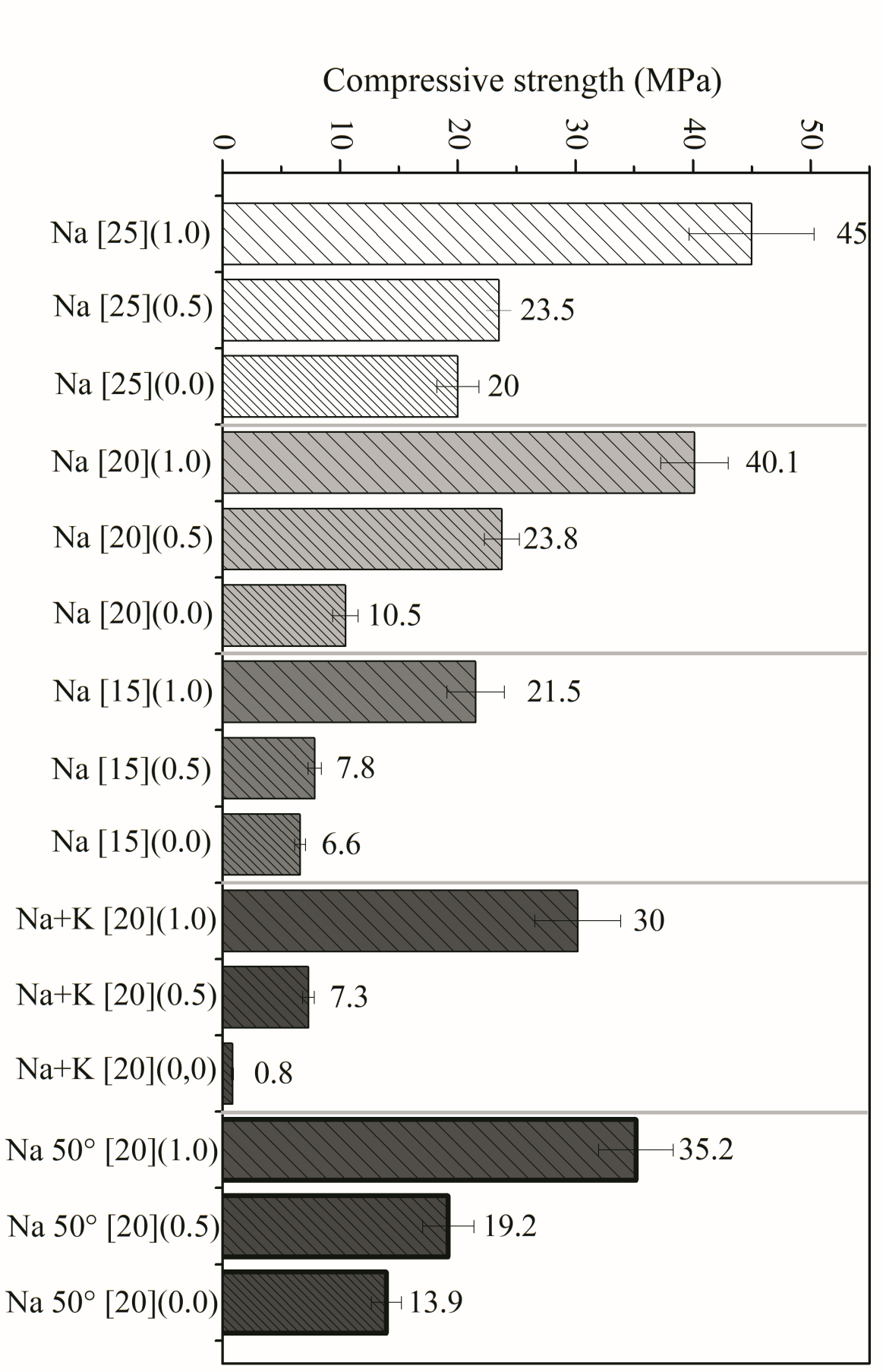
Compressive strength (MPa)
0
10
20
30
40
50
Na [25](1.0)
45
Na [25](0.5)
23.5
Na [25](0.0)
20
Na [20](1.0)
40.1
Na [20](0.5)
23.8
Na [20](0.0)
10.5
Na [15](1.0)
21.5
Na [15](0.5)
7.8
Na [15](0.0)
6.6
Na+K [20](1.0)
30
Na+K [20](0.5)
7.3
Na+K [20](0,0)
0.8
Na 50° [20](1.0)
35.2
Na 50° [20](0.5)
19.2
Na 50° [20](0.0)
13.9

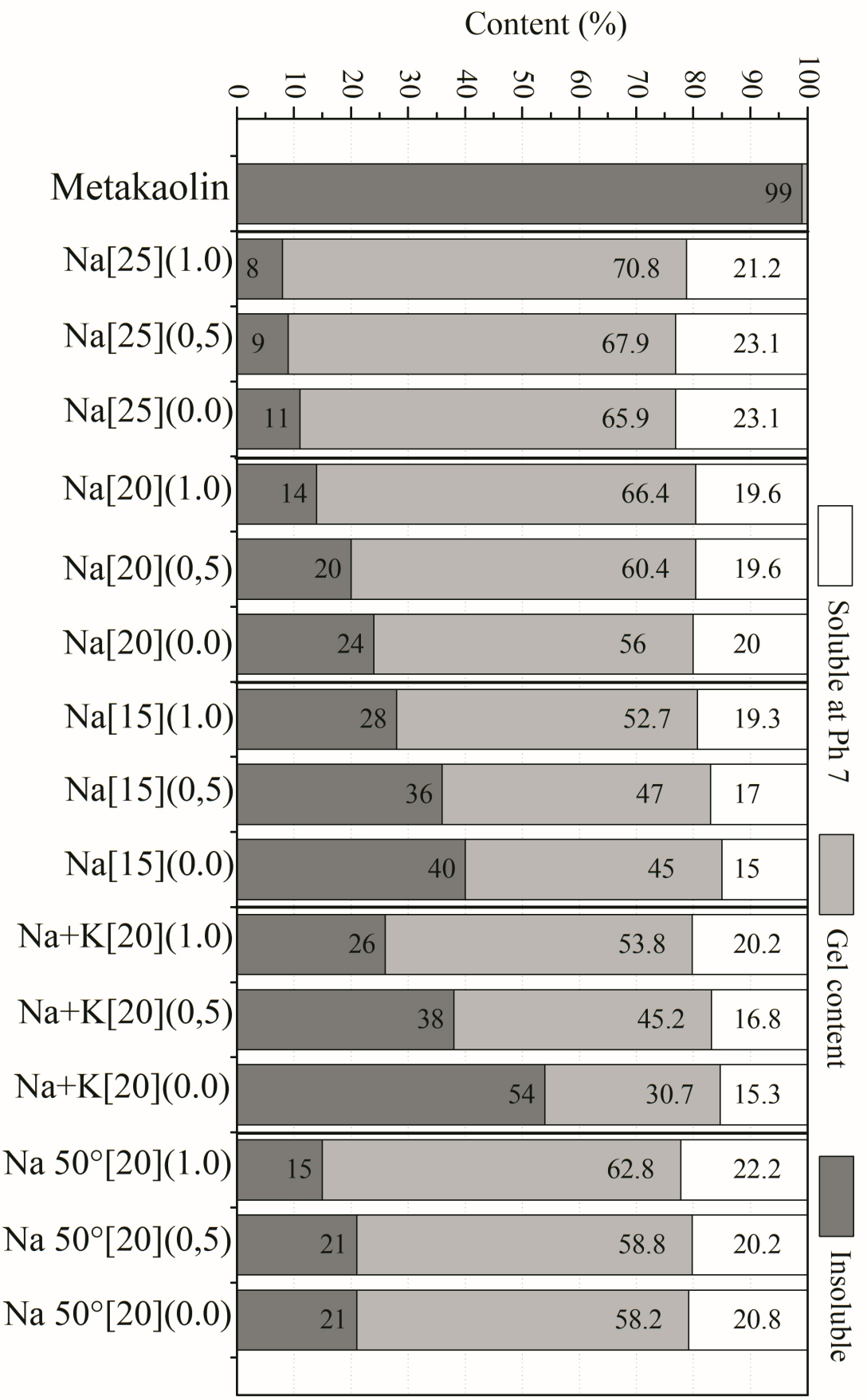
Content (%)
0
10
20
30
40
50
60
70
80
90
100
Metakaolin
99
Na[25](1.0)
8
70.8
21.2
Na[25](0,5)
9
67.9
23.1
Na[25](0.0)
11
65.9
23.1
Na[20](1.0)
14
66.4
19.6
Na[20](0,5)
20
60.4
19.6
Na[20](0.0)
24
56
20
Na[15](1.0)
28
52.7
19.3
Na[15](0,5)
36
47
17
Na[15](0.0)
40
45
15
Na+K[20](1.0)
26
53.8
20.2
Na+K[20](0,5)
38
45.2
16.8
Na+K[20](0.0)
54
30.7
15.3
Na 50°[20](1.0)
15
62.8
22.2
Na 50°[20](0,5)
21
58.8
20.2
Na 50°[20](0.0)
21
58.2
20.8
Soluble at Ph 7
Gel content
Insoluble

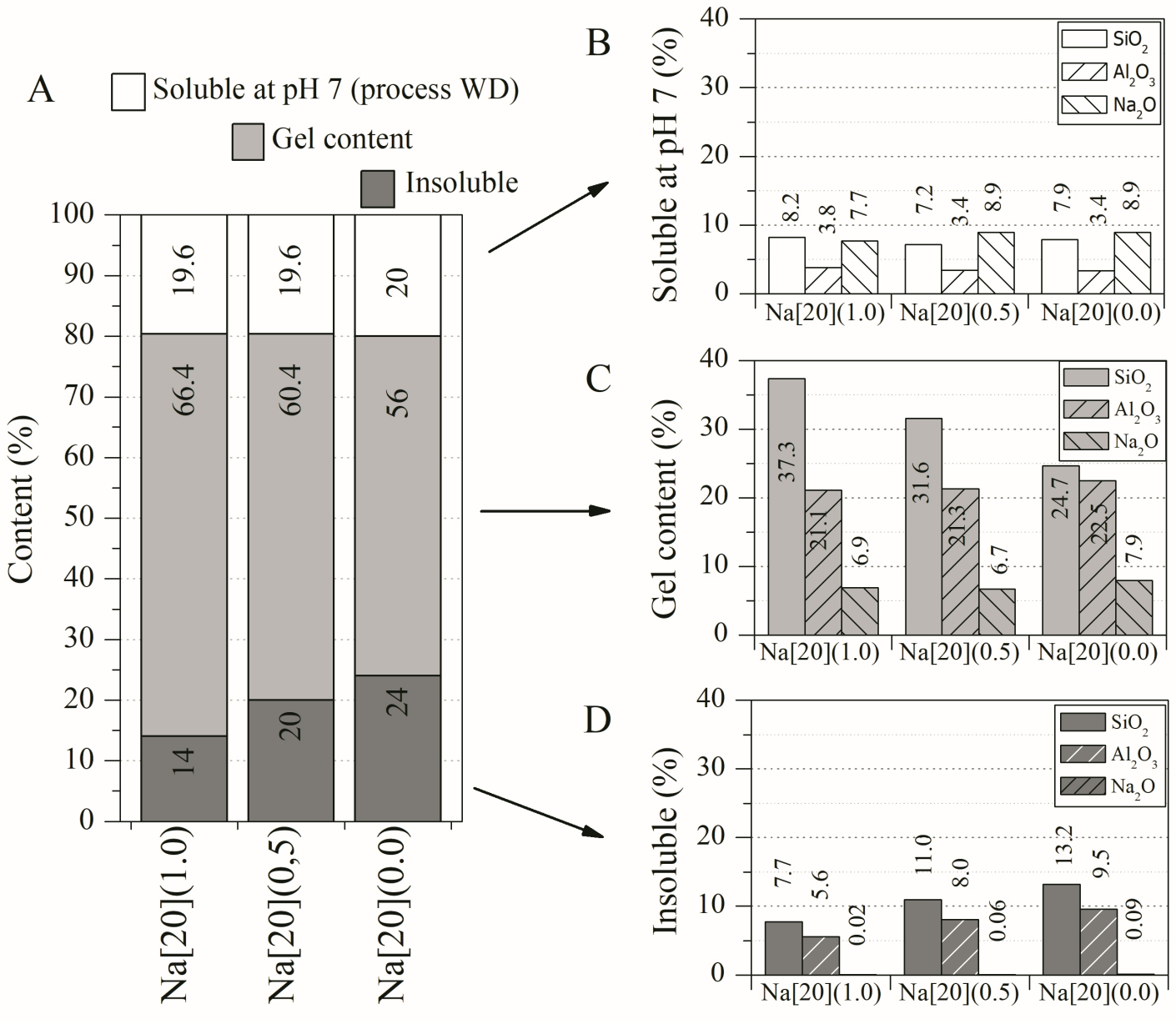
A
Soluble at pH 7 (process WD)
Gel content
Insoluble
Content (%)
100
90
80
70
60
50
40
30
20
10
0
19.6
19.6
20
66.4
60.4
56
14
20
24
Na[20](1.0)
Na[20](0,5)
Na[20](0.0)
B
Soluble at pH 7 (%)
SiO2
Al2O3
Na2O
8.2
3.8
7.7
7.2
3.4
8.9
7.9
3.4
8.9
Na[20](1.0)
Na[20](0.5)
Na[20](0.0)
C
Gel content (%)
SiO2
Al2O3
Na2O
37.3
21.1
6.9
31.6
21.3
6.7
24.7
22.5
7.9
Na[20](1.0)
Na[20](0.5)
Na[20](0.0)
D
Insoluble (%)
SiO2
Al2O3
Na2O
7.7
5.6
0.02
11.0
8.0
0.06
13.2
9.5
0.09
Na[20](1.0)
Na[20](0.5)
Na[20](0.0)

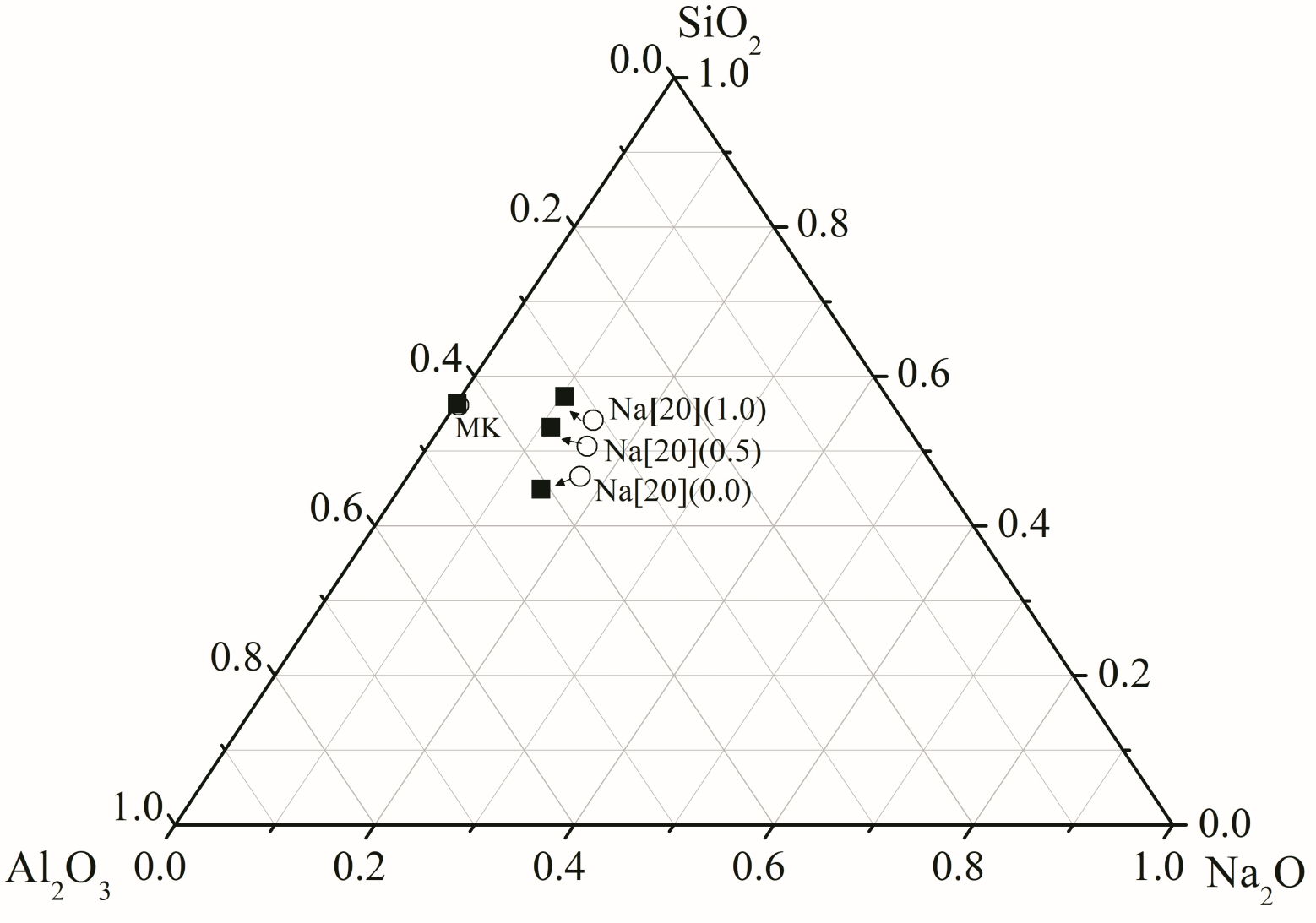
SiO2
0.0
1.0
0.2
0.8
0.4
0.6
0.6
0.4
0.8
0.2
1.0
0.0
Al2O3
0.0
0.2
0.4
0.6
0.8
1.0
Na2O
MK
Na[20](1.0)
Na[20](0.5)
Na[20](0.0)

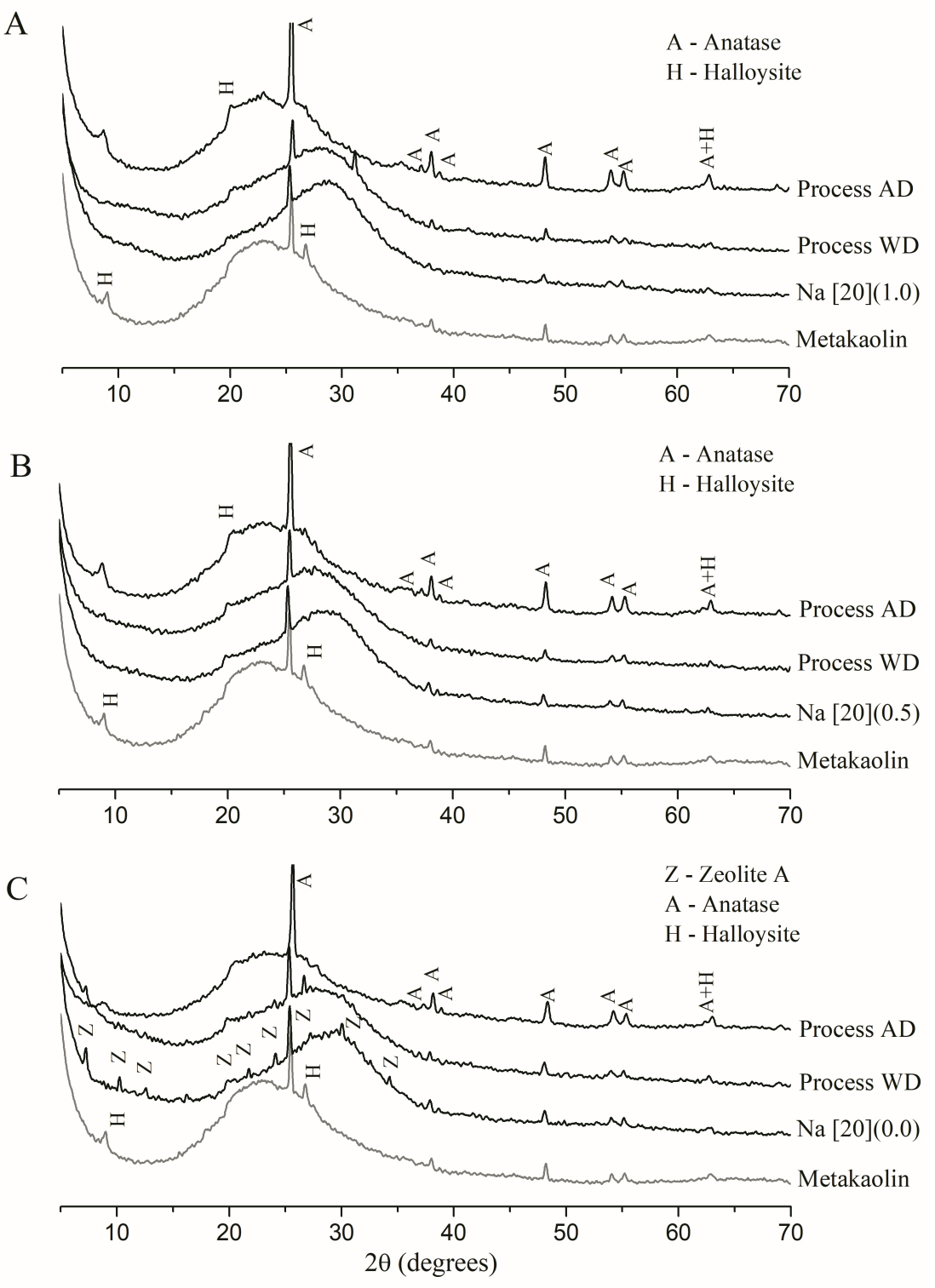
A
A - Anatase
H - Halloysite
Process AD
Process WD
Na [20](1.0)
Metakaolin
B
A - Anatase
H - Halloysite
Process AD
Process WD
Na [20](0.5)
Metakaolin
C
Z - Zeolite A
A - Anatase
H - Halloysite
Process AD
Process WD
Na [20](0.0)
Metakaolin
10
20
30
40
50
60
70
2θ (degrees)

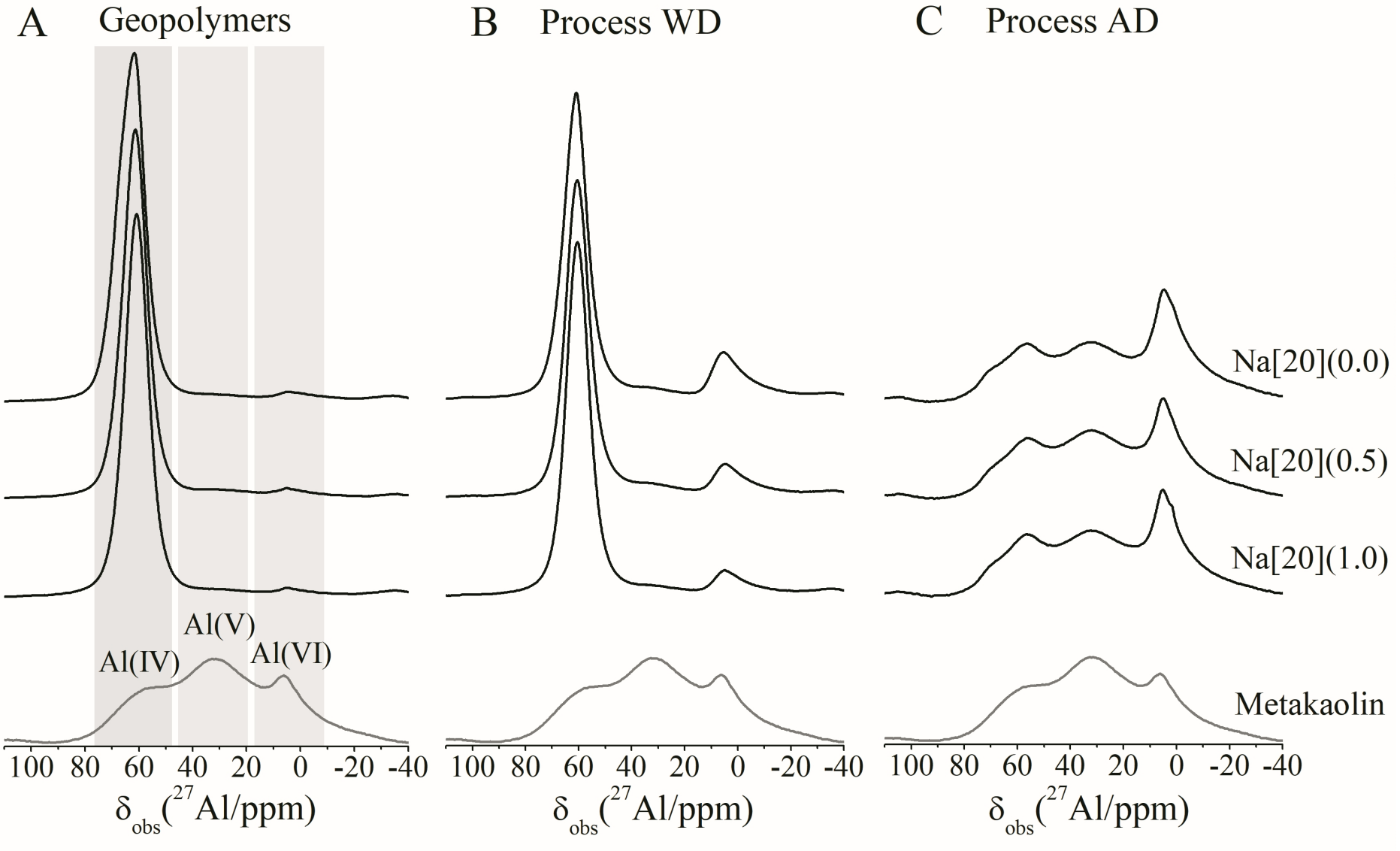
A
Geopolymers
B
Process WD
C
Process AD
Na[20](0.0)
Na[20](0.5)
Na[20](1.0)
Metakaolin
Al(IV)
Al(V)
Al(VI)
100 80 60 40 20 0 -20 -40
δobs(27Al/ppm)

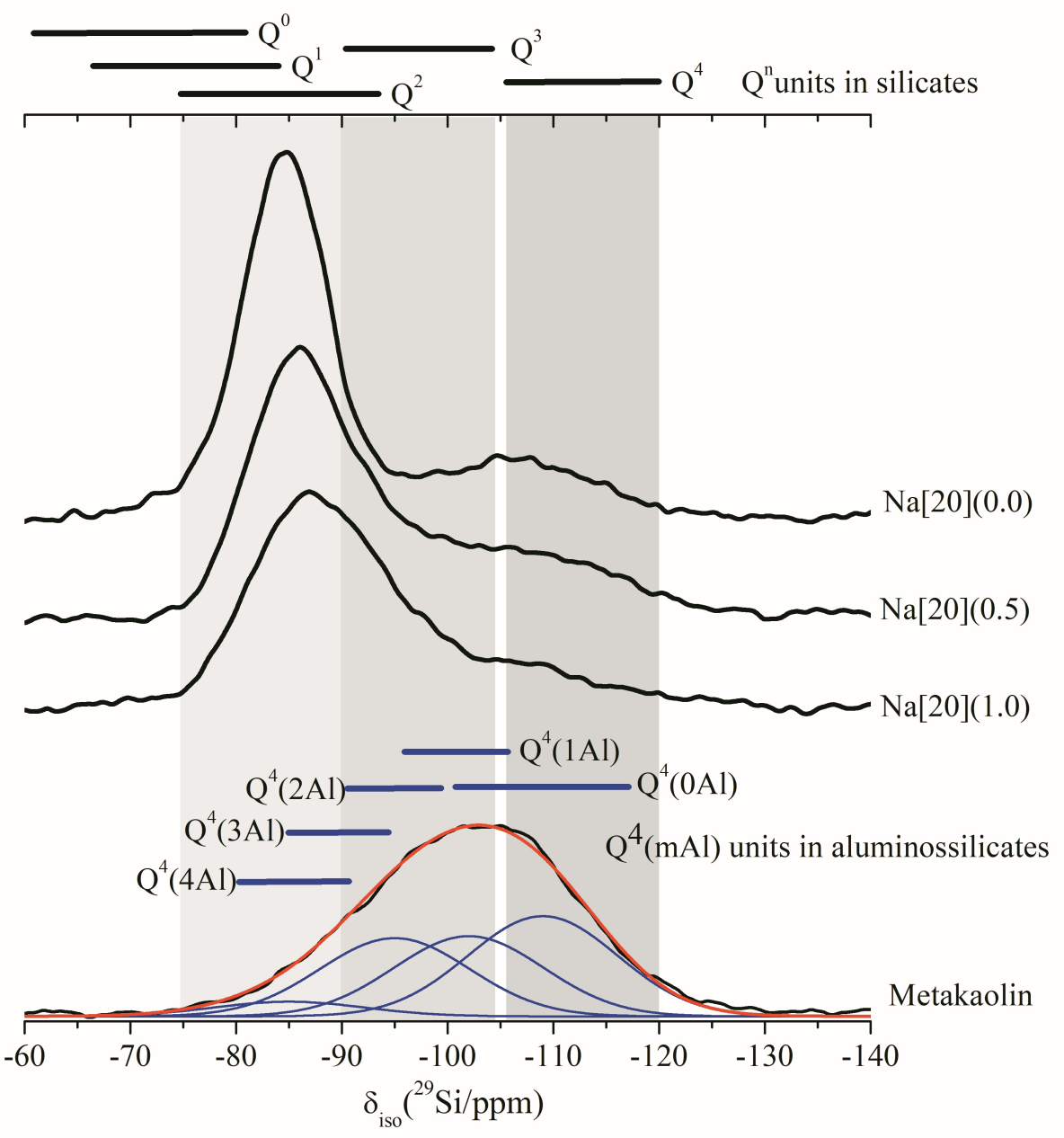
Q0
Q1
Q2
Q3
Q4
Qnunits in silicates
Na[20](0.0)
Na[20](0.5)
Na[20](1.0)
Q4(1Al)
Q4(2Al)
Q4(0Al)
Q4(3Al)
Q4(4Al)
Q4(mAl) units in aluminossilicates
Metakaolin
-60
-70
-80
-90
-100
-110
-120
-130
-140
δiso(29Si/ppm)

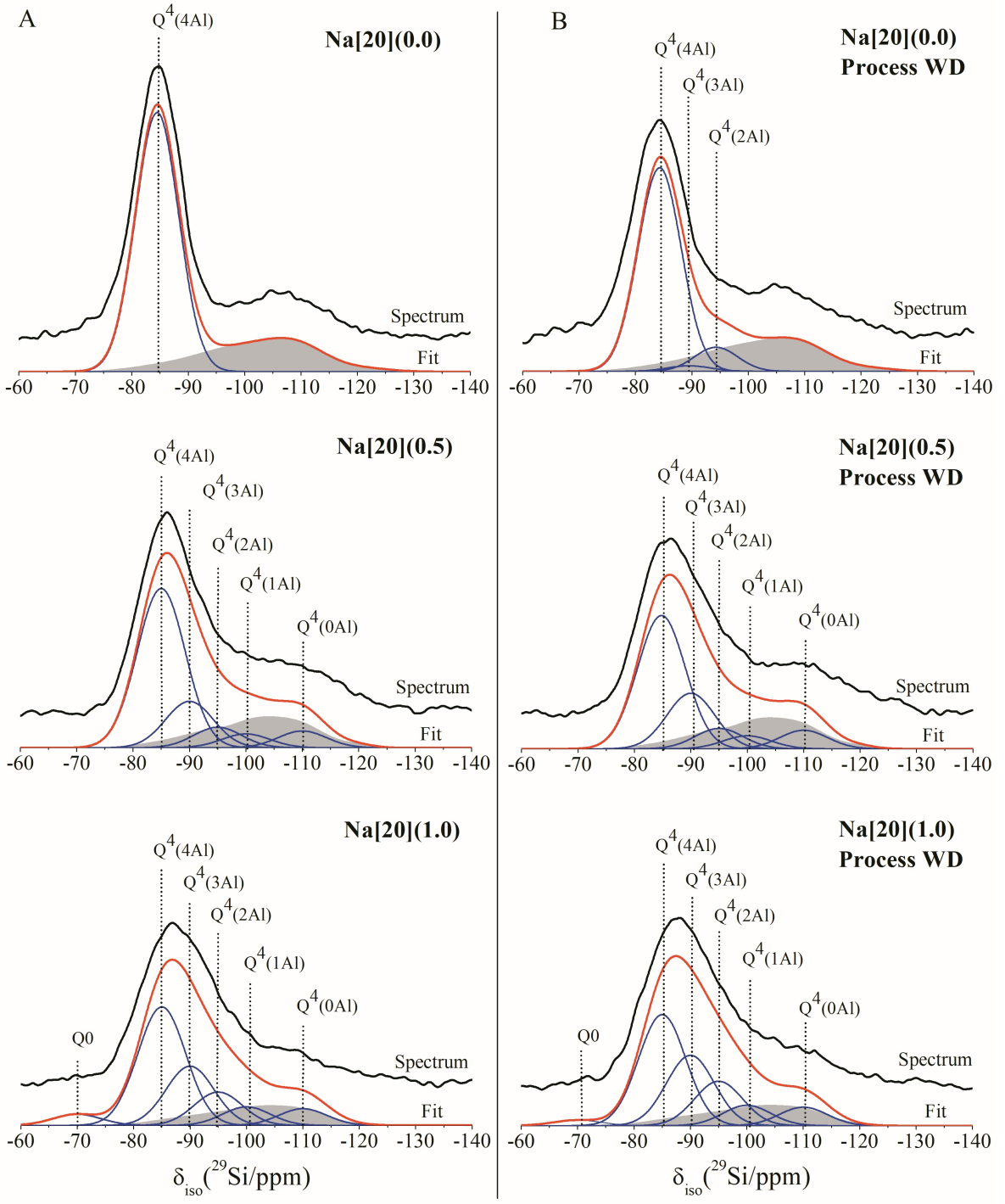
A
B
Na[20](0.0)
Na[20](0.0)
Process WD
Na[20](0.5)
Na[20](0.5)
Process WD
Na[20](1.0)
Na[20](1.0)
Process WD
Q4(4Al)
Q4(3Al)
Q4(2Al)
Q4(1Al)
Q4(0Al)
Q0
Spectrum
Fit
-60 -70 -80 -90 -100 -110 -120 -130 -140
δiso(29Si/ppm)

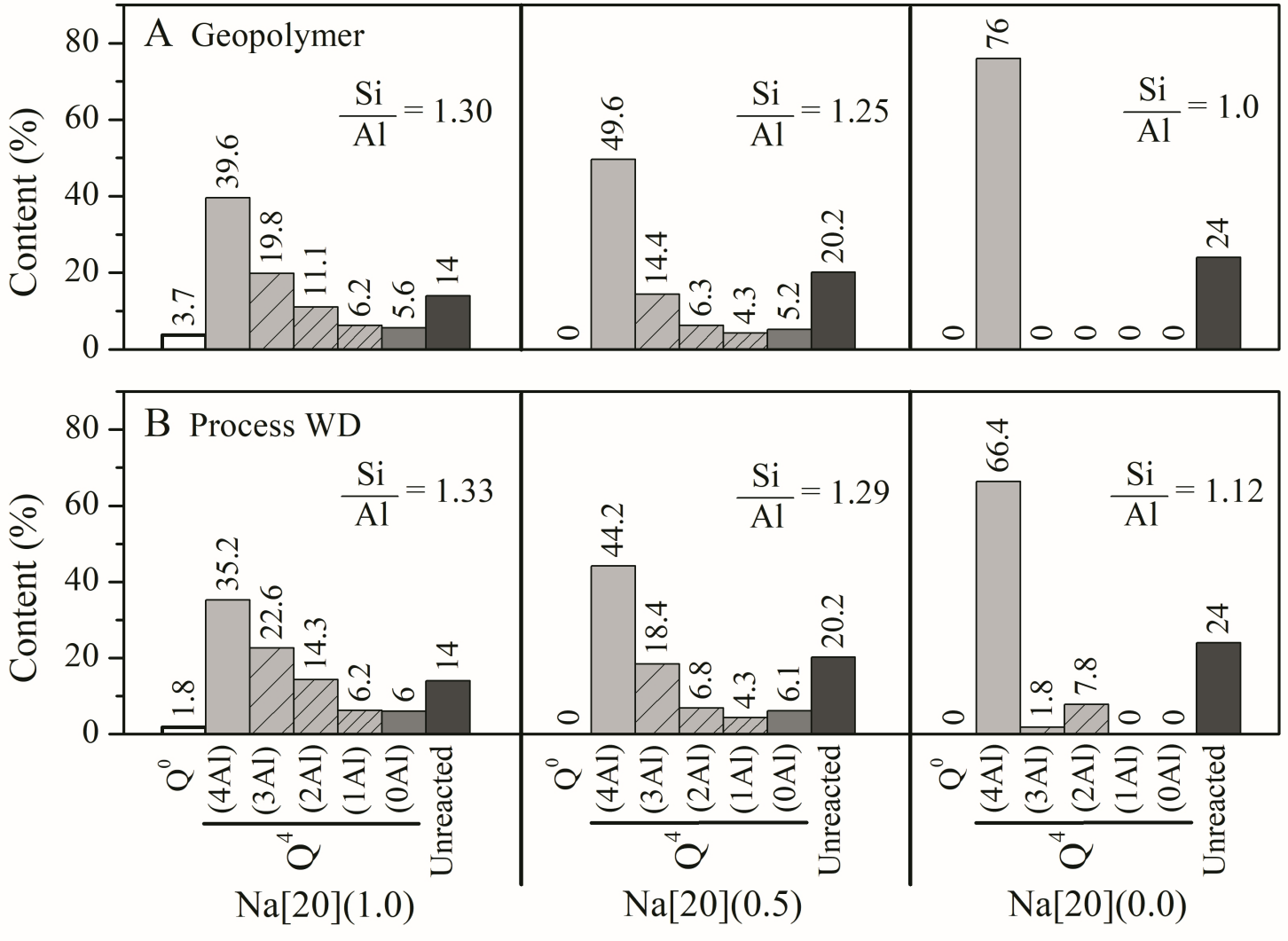
A Geopolymer
B Process WD
Content (%)
Si/Al = 1.30
Si/Al = 1.25
Si/Al = 1.0
Si/Al = 1.33
Si/Al = 1.29
Si/Al = 1.12
3.7
39.6
19.8
11.1
6.2
5.6
14
0
49.6
14.4
6.3
4.3
5.2
20.2
0
76
0
0
0
0
24
1.8
35.2
22.6
14.3
6.2
6
14
0
44.2
18.4
6.8
4.3
6.1
20.2
0
66.4
1.8
7.8
0
0
24
Q0
Q4
(4Al)
(3Al)
(2Al)
(1Al)
(0Al)
Unreacted
Na[20](1.0)
Na[20](0.5)
Na[20](0.0)

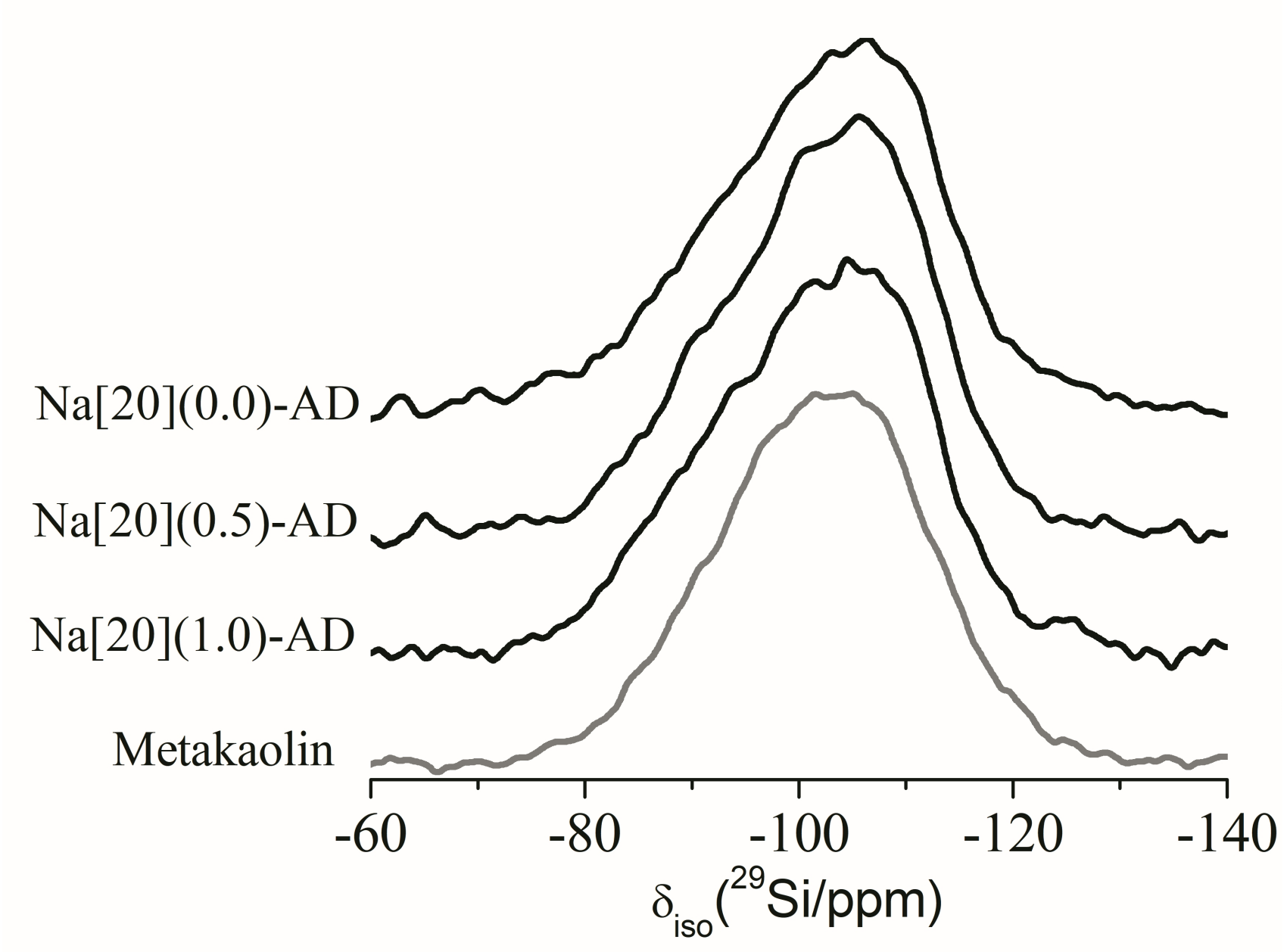
Na[20](0.0)-AD
Na[20](0.5)-AD
Na[20](1.0)-AD
Metakaolin
-60
-80
-100
-120
-140
δiso(29Si/ppm)

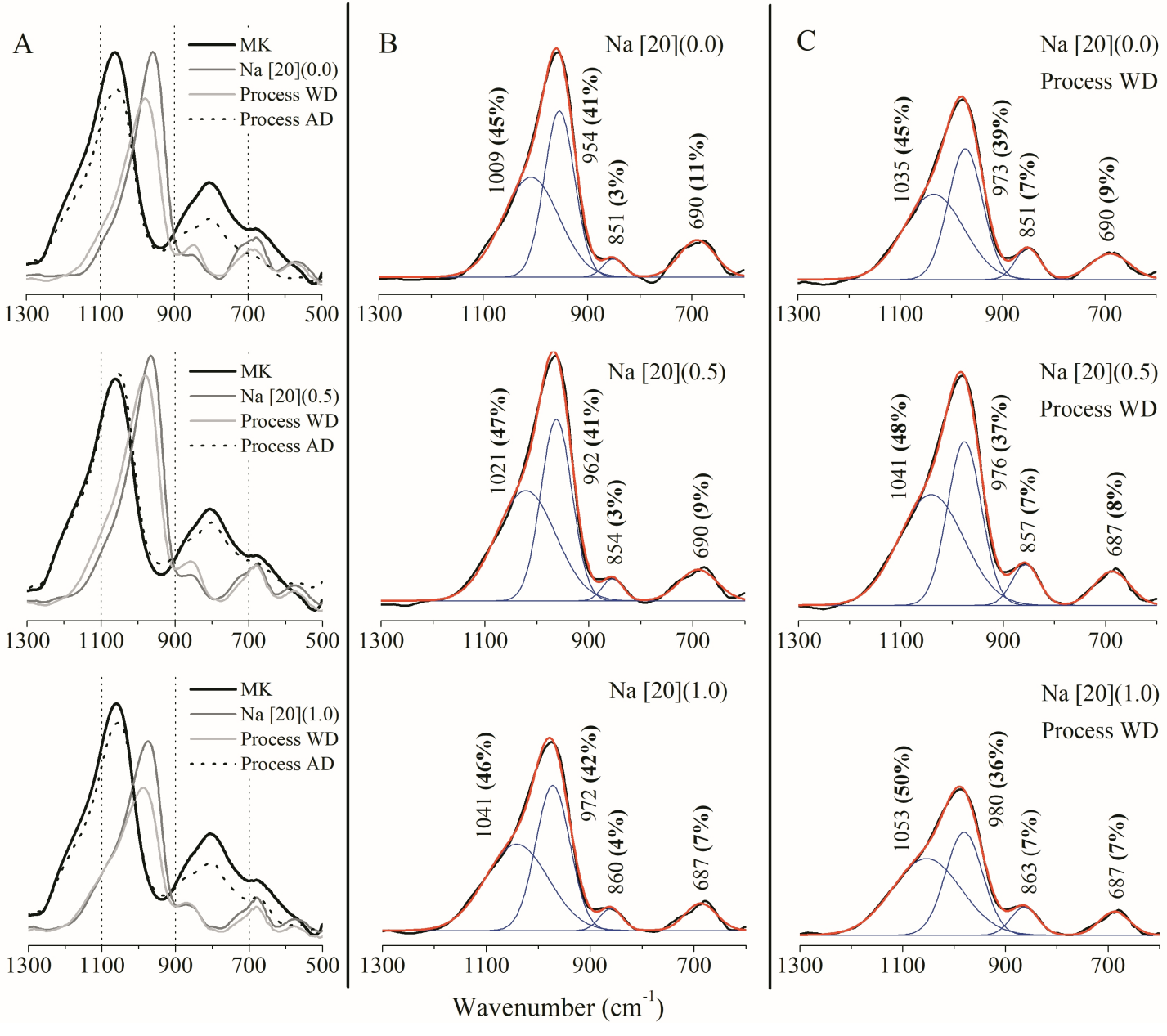
A
MK
Na [20](0.0)
Process WD
Process AD
1300
1100
900
700
500
MK
Na [20](0.5)
Process WD
Process AD
MK
Na [20](1.0)
Process WD
Process AD
B
Na [20](0.0)
1009 (45%)
954 (41%)
851 (3%)
690 (11%)
Na [20](0.5)
1021 (47%)
962 (41%)
854 (3%)
690 (9%)
Na [20](1.0)
1041 (46%)
972 (42%)
860 (4%)
687 (7%)
C
Na [20](0.0)
Process WD
1035 (45%)
973 (39%)
851 (7%)
690 (9%)
Na [20](0.5)
Process WD
1041 (48%)
976 (37%)
857 (7%)
687 (8%)
Na [20](1.0)
Process WD
1053 (50%)
980 (36%)
863 (7%)
687 (7%)
Wavenumber (cm-1)

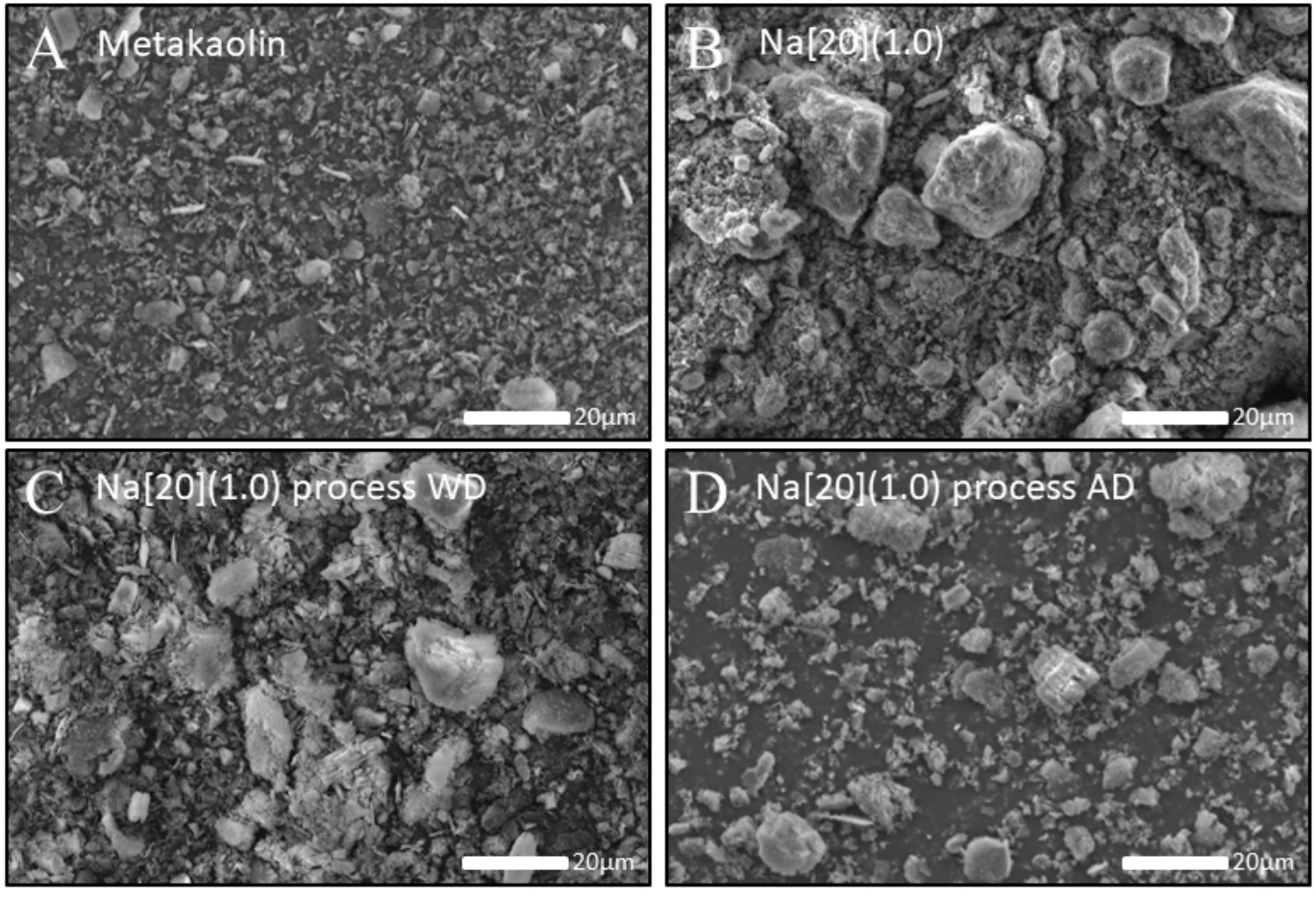
A Metakaolin
20µm
B Na[20](1.0)
20µm
C Na[20](1.0) process WD
20µm
D Na[20](1.0) process AD
20µm